Leveraging place field repetition to understand positional versus nonpositional inputs to hippocampal field CA1

William Hockeimer[1,2,3*], Ruo-Yah Lai[1], Maanasa Natrajan[2], William Snider[1,2], James J. Knierim[1,2,4*]

[1]Krieger Mind/Brain Institute, Johns Hopkins University, Baltimore, MD, 21218

[2]Solomon H. Snyder Department of Neuroscience and Kavli Neuroscience Discovery Institute, Johns Hopkins University School of Medicine, Baltimore, MD, 21205

[3]Current affiliation: Rehab Neural Engineering Labs, University of Pittsburgh, Pittsburgh, PA, 15213

[4]Lead Contact

*Correspondence wih38@upitt.edu; jknierim@jhu.edu

Abstract

The hippocampus is believed to encode episodic memory by binding information about the content of experience within a spatiotemporal framework encoding the location and temporal context of that experience. Previous work implies a distinction between positional inputs to the hippocampus that provide information about an animal's location and nonpositional inputs which provide information about the content of experience, both sensory and navigational. Here we leverage the phenomenon of "place field repetition" to better understand the functional dissociation between positional and nonpositional inputs to CA1. Rats navigated freely on a novel maze consisting of linear segments arranged in a rectilinear, city-block configuration, which combined elements of open-field foraging and linear-track tasks. Unlike typical results in open-field foraging, place fields were directionally tuned on the maze, even though the animal's behavior was not constrained to 1-D trajectories. Repeating fields from the same cell tended to have the same directional preference when the fields were aligned along a linear corridor of the maze, but they showed uncorrelated directional preferences when they were unaligned across different corridors. Lastly, individual fields displayed complex time dynamics which resulted in the population activity changing gradually over the course of minutes. These temporal dynamics were evident across repeating fields of the same cell. These results demonstrate that the positional inputs that drive a cell to fire in similar locations across the maze can be behaviorally and temporally dissociated from the nonpositional inputs that alter the firing rates of the cell within its place fields, thereby increasing the flexibility of the system to encode episodic variables within a spatiotemporal framework provided by place cells.

Introduction

All behavior is embedded within a spatial and temporal framework. In the mammalian brain, allocentric space is represented within a distributed, interconnected network of regions that specialize in different aspects of spatial experience (O'Keefe, 1976; Taube, 1998; Hafting et al., 2005, Alexander and Nitz, 2017; Nitz, 2012; Sharp et al., 1999). This navigation system is critically dependent on the hippocampus, whose pyramidal cells have spatial firing fields that are distributed throughout the environment to provide a continuous representation of position (O'Keefe and Dostrovsky, 1971, O'Keefe 1976). These place cells are thought to form the basis of a cognitive map within which the "items and events of an organism's experience are located and interrelated" (O'Keefe and Nadel, 1978, p. 1) in support of episodic memory.

Neurons within the hippocampus respond to a wide array of sensory and otherwise nonspatial cues, with CA1 being the most studied region. CA1 neurons respond to odors (Wiener et al., 1989; Wood et al., 1999; Wiebe and Stäubli 1999; Komorowski et al., 2009; Allen et al., 2016), tones (Moita et al., 2003; Aronov et al., 2017), textures (Itskov et al., 2011) and tastants (Herzog et al., 2019; Herzog et al., 2020). According to the cognitive map theory (O'Keefe and Nadel, 1978), these variables are represented in the spatial place map to incorporate details about the individual components of an experience and bind them together to form episodic memory traces. Hippocampal neurons also respond to variables that are navigational but nonpositional. For example, neurons have been recorded that respond to heading direction (McNaughton et al., 1983; Wiener et al., 1989; Markus et al., 1995), prospective and retrospective turns or positions (Wood et al., 2000; Ferbinteanu and Shapiro, 2003; Smith and Mizumori, 2006; Ji and Wilson, 2008), entire routes (Grieves et al., 2016), and speed (McNaughton et al., 1983; Czurkó et al., 1999; Maurer et al., 2012; Huxter et al., 2003;

Wiener and Eichenbaum, 1989). These variables relate to navigation, but do not explicitly encode the current position.

In many of the examples above, and related studies, the firing rates of the neurons changed while the locations of the firing field stayed stable (Leutgeb et al., 2005; Herzog et al., 2019; Moita et al., 2003; Wood et al., 2000). It should be noted that in at least one study some place fields shifted their center of mass in response to combinatorial cue changes, although this study also reported in-field firing rate changes as well (Anderson and Jeffery, 2003). These findings led to the hypothesis, termed “rate remapping” (Leutgeb et al., 2005), that stipulates a dissociation between where the neuron fires and the quantitative rate of firing within the field (Shapiro et al., 1997; Manns and Eichenbaum, 2009). The location of the field is used to encode position while the exact firing rate varies as a function of nonpositional cues (so long as the firing rate is maintained above some threshold to indicate the field is active). The common representation, via rate remapping, of both sensory cues and navigational cues unrelated to position suggests that they are both categorized together as nonpositional variables distinct from the positional signal that is the primary (i.e., prerequisite) behavioral correlate of hippocampal firing in rodents.

It is poorly understood how positional and nonpositional inputs are integrated within individual place cells. Place cells with multiple fields in an environment provide an opportunity to study the functional difference between these inputs by allowing a within-cell comparison of multiple nonpositional inputs across multiple place field locations. CA1 neurons have multiple fields under different circumstances, for instance in large environments (Rich et al., 2014; Lee et al., 2020; Park et al., 2011; Harland et al., 2021) or environments with repeated structural elements. The latter, termed “place field repetition” (Spiers et al., 2015, Grieves et al., 2017), is defined as a neuron with multiple spatial firing fields at instances of a repeated structural element or behavioral motif, such as a route, in an environment. For CA1, many different types of repeating track structure can elicit place field repetition, for example multiple boxes arranged in a row (Skaggs and McNaughton, 1998; Spiers et al., 2015; Grieves et al., 2016), a spiral track (Cowan and Nitz 2014), a spiral staircase (Hayman et al., 2011), or an M-maze or hairpin maze (Frank et al., 2000; Derdikman et al., 2009; Singer et al., 2010). Repetition has also been observed outside of the hippocampus, in the entorhinal cortex (Frank et al., 2000), subiculum (Stewart et al., 2014), and retrosplenial cortex (Alexander and Nitz, 2017). Here, we show that repeating fields of the same neuron do not always display the same nonpositional rate modulation, demonstrating that nonpositional cues are dissociable from, and more flexible than, the positional inputs onto place cells in a given environment.

Materials and Methods

Animals and Pre-training

Five Long-Evans rats (3 males, 2 females, 3-6 months old, 325-350 g males, 215-250 g females) were used in the study. Data from male and female rats were consistent with one another and so data from all rats were pooled together (Fig S7). Animals were maintained at 80% of their *ad libitum* weight to provide motivation during the task. Pretraining began once the animal’s weight was near the target weight and its behavior was calm in response to handling. Animals were trained once a day for approximately one hour to run clockwise laps around the perimeter of the track for a separate experiment, receiving liquid reward (~50 µL 1:1 water:Ensure, Abbott Laboratories, Abbott Park, IL). Two rewards were given pseudo-randomly

per lap. Over the course of pre-training the number of laps and time spent in a start box were increased. When the animal reached a performance criterion of 30-60 laps of consistent, motivated behavior, the animal was deemed ready for hyperdrive implantation.

Hyperdrive Construction and Implantation

Custom hyperdrives were implanted over right CA1 (2.5 mm posterior and 2.3 mm lateral to bregma, Fig. S1) in each animal, allowing simultaneous recording of hippocampal ensembles from independently adjustable tetrodes (Wilson and McNaughton 1993). The hyperdrive design consisted of a custom, 3D-printed body with 18 independent microdrives (16 tetrodes plus 2 reference electrodes). Each tetrode was composed of four 0.0017'' diameter nichrome wires coated with VG and HML bonding agents (California Fine Wire Co, CA), twisted together, and heated with a heat gun to bond the insulation. Each tetrode was electroplated to a target impedance of 130 kOhm from a typical starting impedance of 2-3 MOhm using a NanoZ plating system (NanoZ system, Multi Channel Systems, Reutlingen, Germany). The hyperdrive was gas sterilized with ethylene oxide for 12 hours before implantation.

Anesthesia was induced with 4% gaseous isoflurane (1L O_2/min) followed by an injection of ketamine (80 mg/kg) and xylazine (10 mg/kg). Surgical anesthesia was thereafter maintained with isoflurane inhalation (to effect). Marcaine (0.15 cc) or Ropivicaine (0.15 cc) were used as local analgesics applied directly to the skull. Meloxicam (2 mg/kg) was given as an analgesic via IP injection post-op and orally 24 hours after surgery. All animal procedures were approved by the Institutional Animal Care and Use Committee of Johns Hopkins University and complied with National Institutes of Health guidelines.

Electrophysiological Recordings

Tetrodes were advanced ~1.3 mm at the time of surgery and advanced further to the pyramidal layer of CA1 over the course of approximately two weeks using stereotypical changes in the EEG (specifically the theta and sharp-wave signals) as guides. All recordings were performed using a 64-channel Neuralynx Digital SX recording system and Cheetah v5 or v6 software (Neuralynx, Bozeman, MT). Electrophysiological signals were filtered using a finite impulse response (FIR) filter from 600-6000 Hz for tetrodes and 1-300 Hz for the EEG. The low-cut taps for the FIR filter were 32 and 0 and the high-cut taps were 64 and 128, for the tetrodes and EEG, respectively. Thresholds for spike detection were set to a minimum of 50 μV. Spiking data were sampled at 32 kHz with each spike comprising a 1 ms sample (7 samples before the waveform peak, 24 after). EEG data were sampled continuously at 32 kHz.

Spike Sorting

Unit isolation was performed using custom software (WinClust, J.J. Knierim). Spike waveform parameters detected from each tetrode wire were visualized against one another on a two-dimensional plot. Given that the signals from each neuron impinge differently on each electrode wire, the spikes from each neuron appeared as different clusters on the plot. These clusters were manually circumscribed on multiple parameter projections and the intersection of these bounds formed the inclusion criteria for each unit. Each cluster was then subjectively ranked on a five-point scale according to how well it was isolated from both the background noise and other, neighboring clusters. Only clusters with an isolation score of three or better were analyzed further. For each rat, two data sets with the best behavior and highest number of well-isolated clusters were selected for quantitative analysis.

Video Tracking

Tracking of the animal's position was achieved using an LED mount attached to the hyperdrive adapter board. An overhead camera recorded data at 30 fps. Color and luminance thresholds were set each day before the experimental session. Positional information was calculated by taking the center of mass of a luminance-thresholded camera frame, while direction was found using a vector defined by the front and back LEDs (which were colored differently for identification).

Behavioral Apparatus

A novel city-block maze was constructed for these recordings (Fig. 1A). The track consisted of a 0.9 x 0.6 m walled platform with six blocks (18.4 x 18.4 x 15.2 cm) arranged in a 2 x 3 grid. The gaps between the blocks and either the other blocks or the perimeter wall created seventeen alleys (14 x 8.25 cm). An IR emitter/detector (emitter: Honeywell, Charlotte, NC; detector: Lite-On, Taipei City, Taiwan) pair was affixed to both entrances to each alleyway. A lickport connected to a peristaltic pump (Adafruit, New York, NY) was mounted to the wall of each alley with a visible light LED mounted above and a buzzer below the surface of each alley. The hardware and software for each alley were controlled by a separate Arduino Uno (Arduino, Somerville, MA), while the task was controlled by a custom Python program connected to the track via an Arduino Mega and communicating with each alley via the I2C protocol (Moeland et al., 1987)

Behavioral Paradigm

Animals navigated freely within the city-block maze for roughly one hour each day, with 15-20 min of baseline recording in a small holding dish before and after recording. Animals had no prior experience on the interior of the maze before recordings started. Liquid reward (75 μL 1:1 Ensure:water) was dispensed from lickports affixed to the face of each of six blocks defining the interior structure of the maze. When infrared beams detected that the animal crossed the threshold of an alley primed for reward, a light flashed and a tone played while reward was dispensed. Two rewards were available on the apparatus at any one time, with a new reward site selected pseudo-randomly once a primed reward site had been visited. The reward selection was performed such that a new reward site must be at least two alleys distant from the site it was replacing, to encourage sampling of the entire apparatus.

Place Field Detection

Two-dimensional rate maps were created with a bin size of 10 pixels (2.1 cm) and a Gaussian smoothing kernel of 1.5 pixels. To identify place fields, local firing rate maxima were found with a minimum distance of 40 pixels between them and the borders around each were expanded until the firing rate decreased below 20% of the peak rate for each bin of the expanding border. These regions were then passed through two thresholding steps. First, the area of the field had to be ≥ 1% of the walkable track area. Second, the peak firing rate had to be ≥ 1 Hz. Regions around a peak that did not pass these thresholds were not included for analysis; this was done to filter small, weakly active regions. Each field was then iteratively split into smaller fields using a watershed algorithm using skimage.morphology.watershed (subsequently moved to skimage.segmentation.watershed; van der Walt et al., 2014). This splitting process identified all local maxima within the field. For each pair of in-field local maxima, the watershed algorithm expanded the regions around each peak until they collided,

resulting in two potential place fields and the boundary between them. These smaller fields were considered valid if they passed the size and activity thresholds described above and if the firing rate of the boundary between them was not more than 75% of the firing rate of the larger peak. If the smaller fields did not pass these thresholds, they were kept as a single, larger field comprising them both. Each detected field of each neuron was assigned to three possible types of regions: a vertical alley, a horizontal alley, or an intersection. Assignment was determined based on overlap between the area of the field and the area of the track region. If the field overlapped at least 30% of the area of the track region (intuitively, it encroached into an alley at least 30% of the alley's length), then the field was defined as being located in that region. If the field overlapped multiple locations, each overlap location was tested to see if the section of field in that location contained at least 25% of the field's overall firing rate. This was computed by summing all the firing rate values in the bins of the rate map in the region and dividing by the summed rate for the whole field. The field was labeled as being present in any and all locations that passed this measure. A manual curation step was also performed (see "Data Filtering and Pre-processing" below).

Data Filtering and Pre-processing

The rate maps described in the "Place Field Detection" section were created with data that were filtered by running speed with a threshold of 1.5 cm/s. This threshold was chosen based on the structure of the environment, which forced the animal to make frequent turns and therefore had little opportunity to reach high speeds. To be included in the data set, the 95th percentile of the firing rate distribution of two-dimensional rate map bins must be ≥ 1 Hz. The place field detection algorithm required manual curation. Field boundaries that did not correspond to a clear, on-track location of spatially tuned firing were excluded. In particular, periods of off-track exploratory head movements were removed at this step. Fields with boundaries that appeared poorly drawn, typically being overly large, were manually restricted. Importantly, this manual curation only removed poor quality fields, consolidated multiple detected 'fields' that were subjectively better explained by being peaks of the same field, or improved their boundaries; new fields were not created.

Passes through the field were defined as consecutive camera frames within the boundary of the field. Samples that exited the field and re-entered within 2 s were grouped together as part of the same pass through that field. Further, the pass was required to visit at least two points inside the field and at least two of these inside points must have been far enough inside the field that the distance from the closest point of the field border to the visit sample was at least 5% of the distance along the shorter of the length or width of the field. The length was taken as the extension of the field along the y-axis and the width was the extension along the x-axis. Additionally, passes the animal made through each alley were filtered to exclude occasions when the animal turned around without fully traversing the alley. This occurred frequently when the animal appeared to check an alley for reward and leave the way it came if no reward was given. Passes on which a reward was delivered were also removed, in order to remove potential firing rate confounds due to reward. Major analyses were re-analyzed with all trials, rewarded and non-rewarded, to confirm that this did not affect the conclusions of those analyses (Supplementary Table 1). Lastly, fields were excluded if there were fewer than two passes each in both directions through the alley. These preprocessing steps were not applied to the analysis of the number of track regions each field overlapped (see first paragraph of *Place Field Repetition* in Results) because this analysis pertained to the overall size and shape of the field and not the sampling through it.

Each pass was normalized by the mean activity at that location throughout the duration of the session. To do this, the spatial bins visited during the pass were identified and the occupancy-normalized firing rate in each spatial bin was computed using the data from a single pass. This single-pass rate map was normalized by the session-averaged rate map. The normalized pass firing rate was then defined as the mean of all spatial bins of the normalized single-pass rate map. The rationale for this normalization was to control for passes which impinged on different parts of the spatial firing field. For instance, the animal may tend to sample the edge of the field when performing one type of trajectory (e.g., making a right turn from one alley to the next) and the center of the field when performing a different type of trajectory (e.g., moving straight ahead from one alley to the next). This would result in lower firing rates for the former behavior, even if the neuron did not in reality distinguish the two conditions.

As mentioned above, neurons could be classified as present at multiple alleys or intersections if their field overlapped a significant proportion (30%) of that region. For most of the analyses here, fields present at multiple locations were filtered by orientation (vertical or horizontal alleys). All analyses where such orientation-filtering was performed were adjusted for this multiple comparison via a Bonferroni correction.

Quantifying Place Field Repetition

Place field repetition was defined in two ways, operationally and statistically. Operationally, place field repetition was defined as any neuron with two or more fields in a common type of location. The common locations were vertical alleys, horizontal alleys, and intersections. Only alley data were analyzed here, except for the time dynamics data (Fig. 6) which included alleys and intersections. This definition implies that any neuron with three or more fields in alleys was defined as repeating. Therefore, operationally, repetition was multi-fieldedness with the additional criterion that only cells with two fields in differently oriented alleys would not be included. This permissiveness was justified by the wide diversity of multi-field patterns seen in the data (Fig. S3). Because it is not clear what drives repetition, and therefore what should count as repetition, a broad definition was employed to study the widest range of phenomena.

A metric termed the orientation alignment score (OAS) was defined to test whether the apparent repeating patterns present within multifielded neurons were more common than the chance placement of fields would suggest. The OAS was a normalized measure that defined for each neuron how aligned the fields were compared to how aligned they possibly could be. First, the number of fields in vertical and horizontal alleys was defined. Next, the number of fields in the majority class was normalized by the total number of fields, yielding an alignment ratio. Next, this was compared to an *a priori* list of the possible alignment ratios for a cell with a given number of fields. Lastly, the ordinal position of the obtained alignment ratio was normalized by the number of possible alignment ratios for that number of fields.

As an example, consider a neuron with 6 fields, 4 of which are in vertical alleys. This is normalized to yield an alignment ratio of 4/6 = 0.67. Next, this ratio is compared to the list of possible alignment ratios for a neuron with 6 fields, which is [3/6 = 0.5, 4/6 = 0.67, 5/6 = 0.83, 6/6 = 1.0]. For an even number of fields the alignment ratio is minimal at 0.5 and maximal at 1.0. For an odd number of fields it is minimal at ((n+1)/2)/n and maximal at 1.0. The alignment scores cannot be lower than these bounds. In this example the alignment ratio of 0.67 is the

second value in the list, out of four possibilities, so the final OAS value is 2/4 = 0.5. The OAS is minimal at 1/(number of alignment values) (here, 0.25) and maximal at 1.0.

To test for significance, the average OAS was computed across all multifielded neurons. Then, fields were randomly reassigned to neurons while maintaining the true total number of fields and a null OAS computed for each neuron. The average null OAS across multifielded neurons was computed and contributed one point to a null distribution. This was repeated 1000 times and the distribution of averaged OAS values was compared to the empirical average OAS with a one-sided statistical test at alpha = 0.05.

Generalized Linear Model

To test whether individual fields encoded direction or time, generalized linear models (GLMs) were fit to the data. As mentioned elsewhere, if a field spanned multiple regions it was split into the portions on vertical or horizontal alleys separately. All GLM analysis was done in R (R version 4.0.3) using RStudio. GLMs were fit using the *glm* function from the *stats* package (R core team, 2022). The normalized firing rate was used as the dependent variable, with an offset of 1 added to make all values non-zero. Based on the observed skewness in the distribution of firing rates, the Gamma family was used with an inverse link function (this choice of family necessitated the +1 offset mentioned above). Current direction was represented as a binary variable. Models incorporating a time regressor represented time as the timestamp of the beginning of the field traversal. The resulting time series was fit with a natural spline with three knots using the splines package from R (Bates and Venables, 2011).

Likelihood ratio tests (LRTs) were used to test the significance of the model fits. This was done using the *lmtest* package in R (Zeileis and Hothorn, 2021). This test compares a base model to a more complex model containing a variable of interest. More complex models virtually always improve the model fit, and the LRT tests whether this improvement is significant. The two variables tested here, in separate analyses, were current direction and time. It was suspected that in at least some cases the variables were correlated such that apparent effects of directional sampling could be due to time dynamics or, conversely, that apparent temporal dynamics were in fact due to changing biases in directional sampling over time. Therefore, when computing the LRT for the effect of current direction, the base model included a term for time. Conversely, when computing the LRT for the effect of time, the base model included a term for current direction.

The GLM had different sample size requirements than the Mann-Whitney test and therefore some neurons had sufficient sampling for the latter test but not the former. This is because while the Mann-Whitney test estimates one value for the whole population, the GLM includes two terms whose regression weights are calculated along the length of the natural spline with three degrees of freedom. The GLM, therefore, has more parameters to estimate and this requires more data.

Random Forest Classifier

A random forest classifier was used to decode direction from the ensemble firing rates (Breiman, 2001) using the scikit-learn package in Python (Pedregosa et al., 2011). For this analysis, place field boundaries were not used, as the activity of the entire recording ensemble was used regardless of where the cell fired. Behaviors when the animal turned around or was rewarded were removed as in other analyses. For each pass through each alley, a population vector was created. The ith entry of the vector was the normalized firing rate of the ith neuron.

The normalized firing rate was computed as discussed above with the change that the session-wide activity in the alley was used. Each vector was associated with a directional label. The classifier used the population vector of firing rates as the input. Data were filtered by orientation such that direction was decoded from all horizontal alleys separately from the vertical alleys. The out-of-bag (OOB) score was used, as is standard for random forest classifiers. The OOB score is a measure of prediction accuracy based on testing trees on samples which they were not trained on (which occurs due to the bootstrap nature of the training procedure for each tree).

Time Series Interpolation

The time series of each field's activity over time were correlated with one another. Because, in general, each time series had a different length, the vectors were interpolated to equate their sampling. The variability in time series length was a consequence of unequal sampling of each field due to the free foraging nature of the task. 1-D Piecewise Cubic Hermite Interpolating Polynomial (PCHIP) interpolation was used because the fit was monotonic and would not overshoot the underlying signal (Fritsch and Butland, 1984). The implementation used scipy.interpolate.pchipinterpolator in Python (scipy, Virtanen et al., 2020).

Linear Decoder Methods

A linear regression decoder was used to decode position from the ensemble firing rates. Spikes from each neuron were convolved with a Gaussian kernel (sigma = 25 camera frames) to create an instantaneous firing probability distribution. Data were also analyzed using a shorter convolution window (sigma = 8 frames) to test the effect of window size on the results; the pattern of results was not affected by convolution window size. Data were mean centered and normalized using sklearn.preprocessing.StandardScalar. X and Y positions were predicted from the population activity vector at each time point using sklearn.linear_model.LinearRegression. The r^2_score function from scipy.metrics was used to estimate model performance as the amount of variance of the dependent variable (position) explained by the independent variable (population activity vector). Time epochs of alternating training (8000 points) and test (1000 points) windows were created. These windows were interspaced with buffers (500 points) so that the convolution process mentioned above did not cause data leakage. The decoder was trained on all training windows pooled together and tested on all testing windows pooled together. To estimate the variance in the decoder performance, the window boundaries were circularly rotated 1000 times, with shifts drawn from a uniform distribution. For the temporal decoding analysis (Fig 6 F,G), the training windows were used to separately test on the rest of the windows. For the temporal decoding analysis the training windows were 10000 points, the testing windows were 1000 points, and the buffers were 1000 points.

Frequentist Statistical Tests

Mann-Whitney U tests were used as one method to test the directional firing of place fields. The mannwhitneyu function was used from the scipy.stats Python package. T-tests were performed using scipy.stats.ttest_1samp. Ordinary Least Squares (OLS) regression was used to test the correlation within pairs of fields from the same corridor or different corridors (Fig 5). The statsmodels package in Python was used (Seabold and Perktold, 2010). A Fisher Z-test was used as an additional method to test the difference in correlations between the same corridor and different corridor field pairs (Fisher, 1925, p 161-168). The cocor package in R was used for this using the cocor.indep.groups function (Diedenhofen, 2016). A binomial test was used to compare different observed frequencies to those expected by chance. The function used was

scipy.stats.binom_test with a one-sided (greater) test unless otherwise indicated. Chi-square goodness of fit tests were used to test the relative frequencies of vertical versus horizontal repeating fields as well as repeating fields sharing or not sharing directional tuning. The scipy.stats.chisquare function was used. Pearson's chi-square test was used to test group differences between repeating and non-repeating fields for directional tuning and temporal dynamics (in separate tests). The scipy.stats.chi2_contingency function was used for this. Hartigan's dip test was used to test whether the route response correlation distribution was not unimodal (Fig 5G). The 'diptest' package in R was used (Maechler, 2021). Data are shown as mean ± standard deviation, unless otherwise noted.

Shuffling Tests

For the same corridor / different corridor analysis, the labels of each pairwise comparison were pooled across the dataset. On each iteration, the labels were reassigned to the groups while preserving the sample sizes (same corridors = 54 pairs, different corridors = 155 pairs). Next, ordinary least-squares regression was performed and the difference in r^2 values for OLS_{same} Tand $OLS_{different}$ was stored as one entry in the null distribution. The 95th percentile of this distribution was compared to the real difference in r^2 values between the groups.

Results

Hippocampal CA1 cells were recorded as rats navigated a novel city-block maze for pseudo-randomly delivered reward (Fig. S2). The track consisted of seventeen interlocking alleys and twelve intersections between them (Fig 1A, B). Each recording day consisted of a single behavioral session, typically one hour in duration. A baseline period, in which the rat was confined to a small holding dish next to the maze, was recorded immediately before and after the experimental session for at least 15 minutes each. On average, 14.7 cells per session (5-35 cells) were recorded that met the inclusion criteria for detailed analysis (see Methods).

Place Field Repetition

Neurons with multiple fields at similar types of locations, termed "repeating place cells" (Spiers et al., 2015), were observed (Fig. 1C). Fields repeated at alleys and intersections within the maze (Fig. 1A). A repeating place cell was defined operationally as any neuron with two or more place fields in a common type of location: vertical alley, horizontal alley, or intersection. This criterion did not penalize cells with violations of a repeating pattern, for instance two fields in vertical alleys and one in a horizontal alley. This was justified by the complex nature of the repeating phenomenon observed (Fig. S3). Repeating fields were equally likely to be in vertical or horizontal alleys (167 horizontal vs 146 vertical fields, Chi-square goodness of fit, compared to a null distribution of equal numbers of horizontal and vertical fields, $X^2(1) = 1.41$, $p = 0.235$). Each repeating cell had up to seven fields, suggesting that repetition was spatially gated, as no cell had fields at each alley (mean number of repeating fields = 3.55 ± 1.46 fields; Fig. 2B). Many cells had fields that overlapped multiple regions, for example fields which curled around the corner of a block (71.89% of fields in one alley; 22.7% of fields in two alleys; 5.1% of fields in three alleys; 0.4% of fields in four alleys). These cases were assigned to the more general three categories (vertical alley, horizontal alley, and intersection) by splitting fields based on the alleys they overlapped and recombining based on orientation (see Methods). Traditional, single-

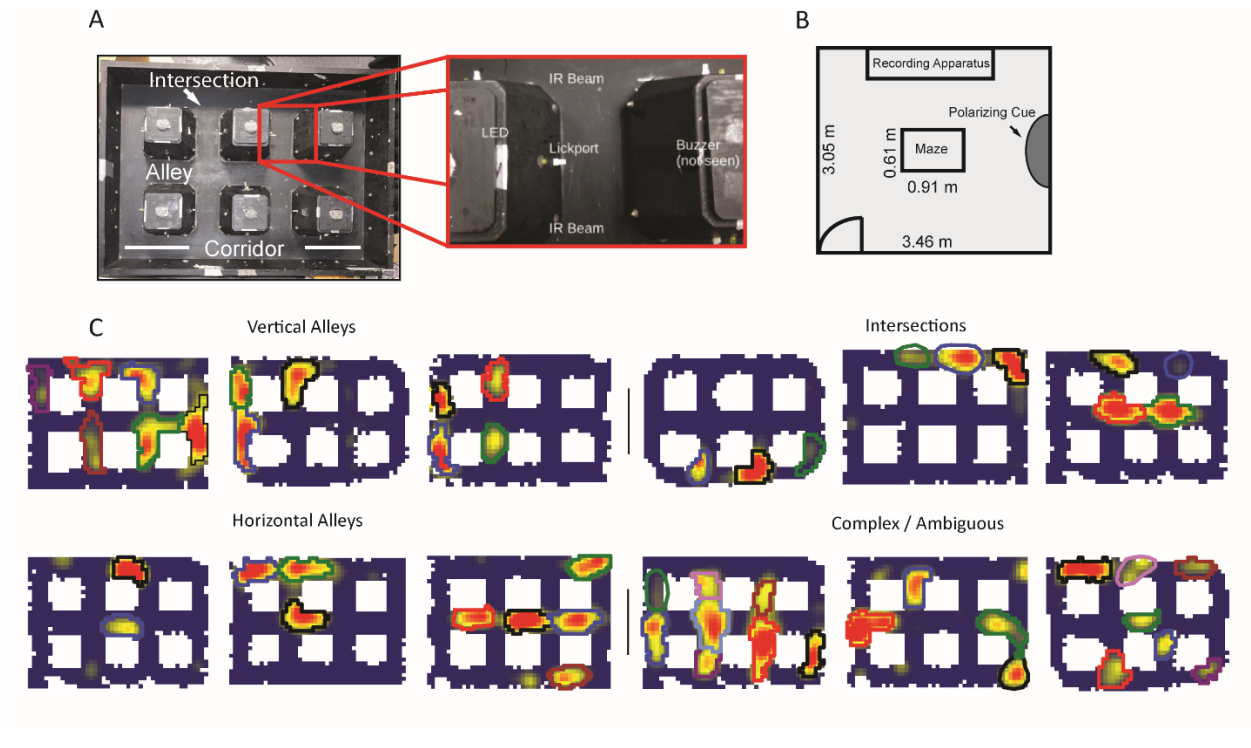

Figure 1 – Apparatus and examples of place field repetition. **A.** Left, top-down view of city-block maze. Perimeter walls (15.2 cm high) enclose an area 60.96 cm x 91.44 cm. Six square obstacles (19.1 x 19.1 cm, 15.2 cm tall) define seventeen alleys in their interstitial spaces along with twelve intersections. Track regions were defined as vertical alleys (oriented north-south), horizontal alleys (oriented east-west), or intersections. Right, enhancement showing an individual alley. An IR emitter and detector pair was affixed to either entrance of the alley. In the center of the alley was a lickport with a visible light LED above. A buzzer was placed under each alley. Lickports here have been extended to make them more visible. **B.** Schematic of recording room and behavioral apparatus. The city-block maze was in the same room as the recording apparatus. A black, floor-to-wall curtain that was gathered together, forming a band along the east wall, served as a polarizing cue. **C.** Examples of repeating fields grouped into four subjective categories: repeating in vertical alleys, repeating in horizontal alleys, repeating in intersections, and complicated or ambiguous patterns of repetition. Spatial bins from off-track sampling were removed from these figures and from quantitative analyses of the place fields. Each identified subfield is outlined in a separate color.

field place cells were also observed in these data as expected (60/179 units). Place field repetition was not driven by the presence of poorly isolated units that combined multiple fields into one “cell”, as there was no significant difference in cell quality between repeating and non-repeating neurons included in the analysis (Mann-Whitney $U = 3214$, $p = 0.1$) .

Place cell repetition was quantified by analyzing the degree to which fields of multi-fielded cells were aligned in alleys of a common orientation. The rationale for this approach was that given the effect of head direction on repetition (Grieves et al., 2016, Harland et al., 2017), cells repeating in response to a preferred local pattern of borders (or the paths available around such borders) would manifest as cells with fields aligned in alleys of a common orientation. First, the distribution of field alignment scores was calculated for each multi-fielded neuron as the sum

of fields aligned in a common orientation divided by the total number of fields (Fig. 2C). This distribution was skewed towards 1.0, suggesting that fields tended to share an orientation. An

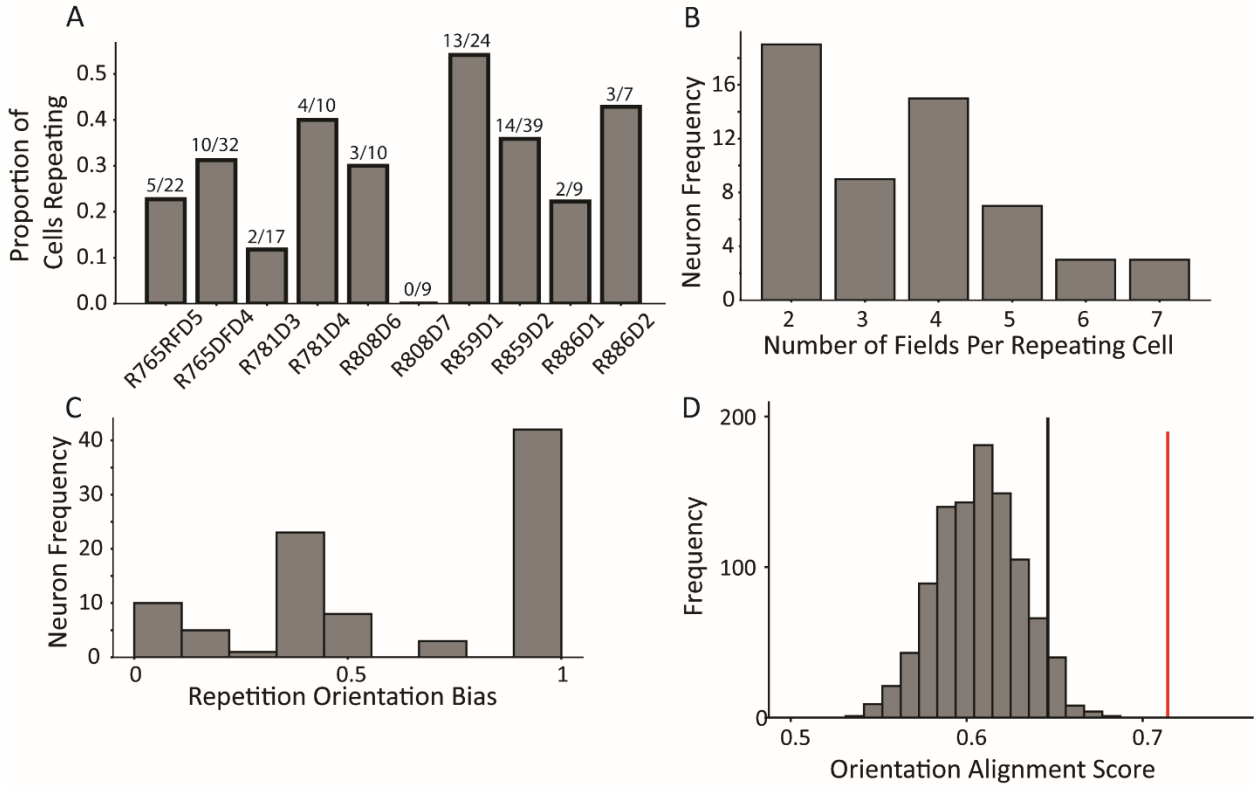

Figure 2 – Characterization of repetition. **A.** The frequency of place field repetition across days and rats as defined operationally (two or more fields in a common location). Each bar shows the proportion of well-isolated cells with on-track firing that was repeating, from ten datasets across five rats. **B.** The distribution of number of fields within repeating cells. Repeating cells had between two and seven detected fields, with half of cells displaying 4 or more fields. **C**. The orientation bias among repeating fields in alleys. Cells were assigned an 'orientation bias score' by taking the ratio between the maximum number of fields sharing a common orientation and the total number of fields. **D.** To quantify repetition, the orientation alignment score (OAS) was defined. The metric first defines the degree of alignment of the fields of a cell, and then expresses that as a percent along the range of possible alignments for that given the number of fields the cell had (see Methods). The y-axis indicates frequency of shuffles of the entire population that that had the average OAS indicated on the x-axis. The mean of the population 0.71 (red) was greater than the 95th percentile of a shuffle distribution (0.64, black).

orientation alignment score (OAS) was defined as the percentage of maximal field alignment given the number of fields the cell had (see Methods). The mean OAS of multi-fielded cells was significantly greater than expected by chance (mean = 0.71, 95th percentile shuffle = 0.64, Fig. 2D). This result demonstrates that multiple fields of a neuron tend to share a positional input that instructs them where to fire. If they did not share such a positional input, their spatial distribution would be random across the track. The fact that the distribution of multiple fields instead respects the orientation of the alleys suggests that there is a common signal that influences their position.

Directionality of CA1 Place Fields

Place fields are known to be directional when rats run on linear tracks or display other types of one-dimensional, stereotyped behavior, but they are much less directional when rats

perform more unstructured, 2-dimensional behavior in open-field foraging (Markus et al., 1995; McNaughton et al., 1983; Navratilova et al., 2012). Because our city-block maze was a hybrid of these types of tasks (i.e., rats ran in two dimensions searching for pseudo-random reward like open-field foraging, but their trajectories were constrained to orthogonal directions by the city-maze architecture), it was of theoretical interest to determine whether place fields were directional in the maze. Continuous, two-dimensional travel through the maze was parameterized according to which alley the rat currently occupied. The current direction was defined based on the overall direction of travel through the alley, as opposed to the instantaneous heading direction. For example, if the animal entered a horizontal alley from the west entrance and exited from the east entrance, then the activity during the time spent in that alley would be classified as “east” regardless of the moment-by-moment head direction (the cardinal directions are defined operationally relative to the camera image, not relative to a geomagnetic compass). First, rate maps were created and filtered by travel direction to yield four rate maps based on each cardinal direction (Fig 3A). These rate maps revealed place fields with firing rates that qualitatively varied as a function of direction. For example, for neuron 1 of Figure 3A, fields 2 and 3 fired more strongly when the animal traveled from east to west, whereas field 1 seemed untuned to travel direction (north and south rate maps are not shown). Further, field 2 not only fired more strongly but shifted its center-of-mass when the animal traveled west. Neuron 2 had multiple firing fields in vertical alleys or intersections. Field 1 fired when the animal was travelling south but was virtually silent when travelling north; field 2 fired more strongly when the animal travelled north than south; and field 3 appeared untuned to travel direction. Neurons 3 and 4 provide similar examples.

The directional firing of each field was quantified. Fields were filtered such that (a) there were at least two passes in each direction and (b) passes in which the rat was rewarded or did not fully traverse the alley (i.e., the rat turned around) were excluded. The firing rate assigned to each pass for a neuron was computed as the mean of the firing rate over the length of the pass, normalized by the session-averaged rate map for that alley (i.e., the pass was normalized by its location within the field). This normalization was done to correct for passes that might have elicited different firing rates simply because the rat may have traversed different portions of the field during different passes. This is a particular concern when analyzing directional variables, because the rat may be biased to run a certain way through the alley when performing a specific behavior (e.g., it may run closer to the east wall before making a right turn and closer to the west wall before making a left turn).

Across the population, a significant subset of fields was directionally tuned (Fig 3B; 93/310 fields passed a Mann-Whitney test per field; binomial test, $p = 3.6 \times 10^{-45}$). The mean difference in normalized directional firing was 1.67 ± 2.20 for fields that passed the Mann-Whitney test and 0.69 ± 0.72 for those that did not. In other words, directional fields had a difference in normalized firing that was two-thirds more than their mean firing. The directionality of individual fields was corroborated by a generalized linear model (GLM) analysis. A field may appear directional due to non-specific changes over time that happen to correlate with biases in behavioral sampling. To account for this, the GLM was first fit with a term for time (base GLM) and then a term for direction was added (alternative GLM). These two models were compared via a likelihood ratio test (LRT) to determine whether the addition of current direction in the model resulted in a significant improvement in the model fit over and above the explanatory power of time. This analysis identified a subset of fields with a significant effect of current

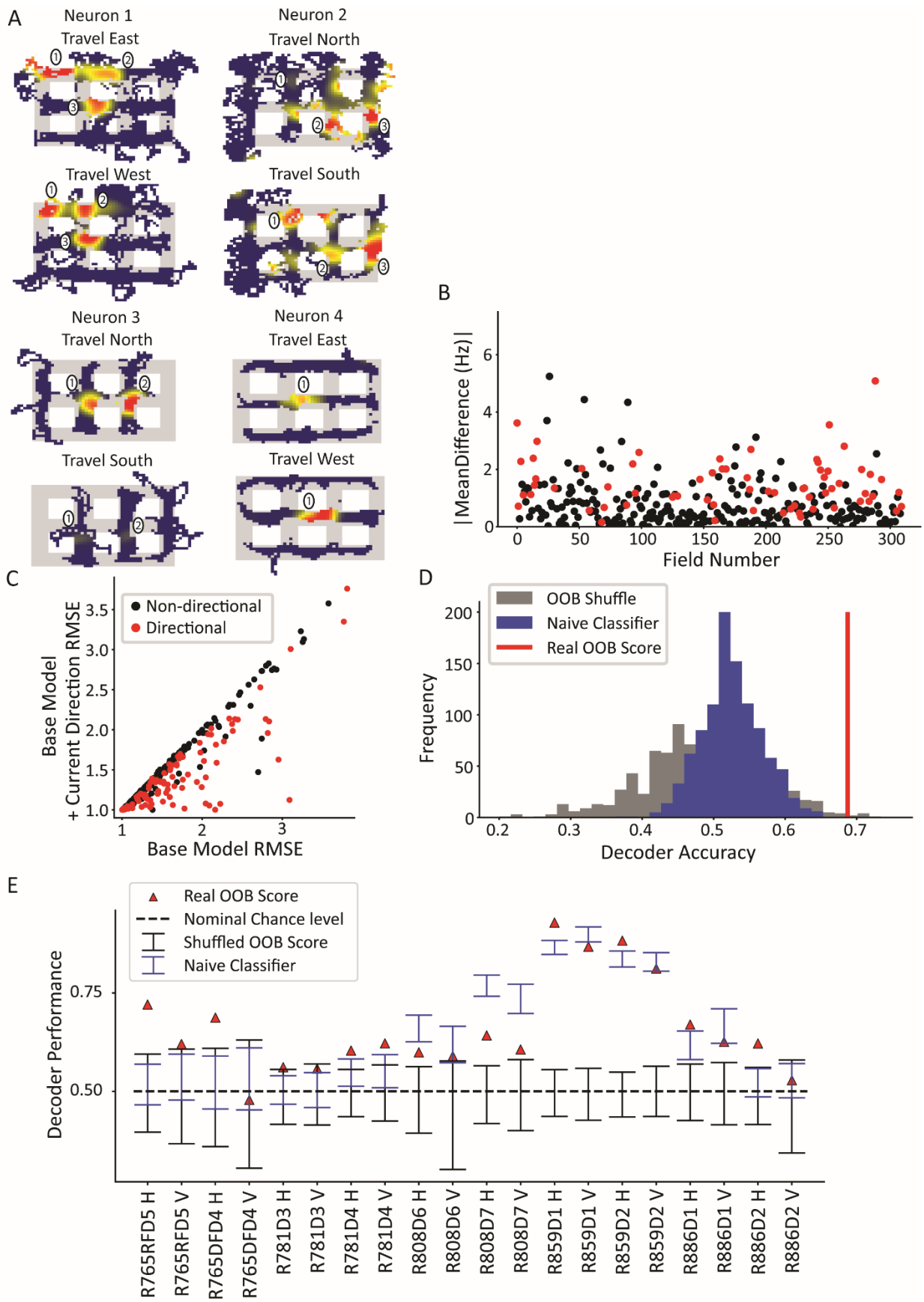
A
Neuron 1
Travel East
Neuron 2
Travel North
Travel West
Travel South
Neuron 3
Travel North
Neuron 4
Travel East
Travel South
Travel West
B
|MeanDifference (Hz)|
Field Number
C
Non-directional
Directional
Base Model
+ Current Direction RMSE
Base Model RMSE
D
OOB Shuffle
Naive Classifier
Real OOB Score
Frequency
Decoder Accuracy
E
Real OOB Score
Nominal Chance level
Shuffled OOB Score
Naive Classifier
Decoder Performance
R765RFD5 H
R765RFD5 V
R765DFD4 H
R765DFD4 V
R781D3 H
R781D3 V
R781D4 H
R781D4 V
R808D6 H
R808D6 V
R808D7 H
R808D7 V
R859D1 H
R859D1 V
R859D2 H
R859D2 V
R886D1 H
R886D1 V
R886D2 H
R886D2 V

Figure 3 – Directionality of place fields in the city-block maze. **A.** Examples of directional place fields. Only unrewarded, straight-through traversals were included for these rate maps and subsequent analyses. Top left, example neuron with east- and west-oriented alley traversals separated into rate maps (north and south rate maps not shown here). Fields 2 and 3 fired more strongly for west over east, while field 1 was untuned. Top right, cell with at least five firing fields in vertical alleys, three of which are labeled. Field 1 preferred south, while field 2 preferred north. Field 3 was untuned. Bottom left, cell with two fields in vertical alleys of adjacent corridors. Both fields fired more strongly when the animal traveled north. Bottom right, cell with single field that fired more strongly when animal traveled west. **B.** The directionality across population of fields. For each field in an alley with sufficient sampling, passes were orientation-filtered. The absolute mean difference in firing rate was computed between directions. A significant number of fields were directional (93/310 field portions, binomial test, $p = 3.6 \times 10^{-45}$, FWER-adjusted alpha = 0.05). Two outliers were removed from the visualization (but not the statistics): Field 132, normalized Hz = 19.08 (significant) and Field 213, normalized Hz = 9.52 (significant). **C.** Generalized linear models were fit to the orientation-filtered data from each field. Points labeled in red were significant according to an LRT between the base and directional GLMs. Root mean square error (RMSE) is shown. The current direction model better explained the data in a significant number of cases (103/297 field pieces, binomial test, $p = 4.53 \times 10^{-57}$, FWER-adjusted alpha = 0.05. One outlier was removed from visualization but not statistics with base RMSE = 4.72, current direction RMSE = 4.67, not significant. **D.** Example random forest decoder results for a single orientation-filtered dataset. A random forest classifier decoded current direction from the population firing rates on each day of recording separately. Alleys were divided into horizontal and vertical alleys and the traversals within them pooled, yielding two data points for each recording day. Random forests with shuffled labels (black) and naïve classifier (blue) were created and the empirical performance (red) was defined as significant if it exceeded the 95th percentile of both control distributions. **E.** Random forest classification performance across 10 days of recording, broken down by alley orientation. The classifier was able to consistently extract a directional signal from 10/20 datasets (binomial test, $p = 1.13 \times 10^{-8}$, FWER-corrected alpha = 0.05).

direction (Fig 3C, 103/297 fields, binomial test $p = 4.53 \times 10^{-57}$; note that the total number of fields, i.e. the denominator, is different here than for the Mann-Whitney test due to the sampling requirements of the two tests (see Methods)).

Next, the CA1 ensemble was tested for directionality at the population level. A random forest classifier was used to decode the current direction from the population vector of average firing rates (Fig 3D). The average firing rate for each neuron was computed for each pass through an alley and labeled with the direction of travel for that pass. Data from vertical and horizontal alleys were classified separately and the out-of-bag (OOB) score (mean = 0.68 ± 0.13) was used as the performance metric. Two controls were used to judge the statistical significance of the performance of the classifier. The first method shuffled the trial labels with respect to the population vectors and the classification was repeated using the (shuffled) OOB score as the performance metric. The second method was a naïve classifier that made a class label prediction in proportion to the behavioral sampling bias in favor of that directional label. The rationale for the naïve classifier test is that a real classifier could potentially utilize class imbalances (e.g., bias to travel north through a given alley) and consistently guess the majority class to achieve above-chance performance. The naïve classifier mimics this strategy by guessing, for each alley traversal, direction labels in proportion to their behavioral sampling frequency over the entire session. The real performance of the classifier was judged significant for each session if it exceeded the 95th percentile of each test. The random forest classifier successfully decoded direction from the population activity in 10/20 orientation-filtered datasets (binomial test $p = 1.13 \times 10^{-8}$, FWER-corrected alpha = 0.05, Fig 3E). On a day-by-day basis, the classifier performance was variable. This may have been caused by differences in cell yield – some days only contained a few cells, which would lead to poorer spatial coverage of the

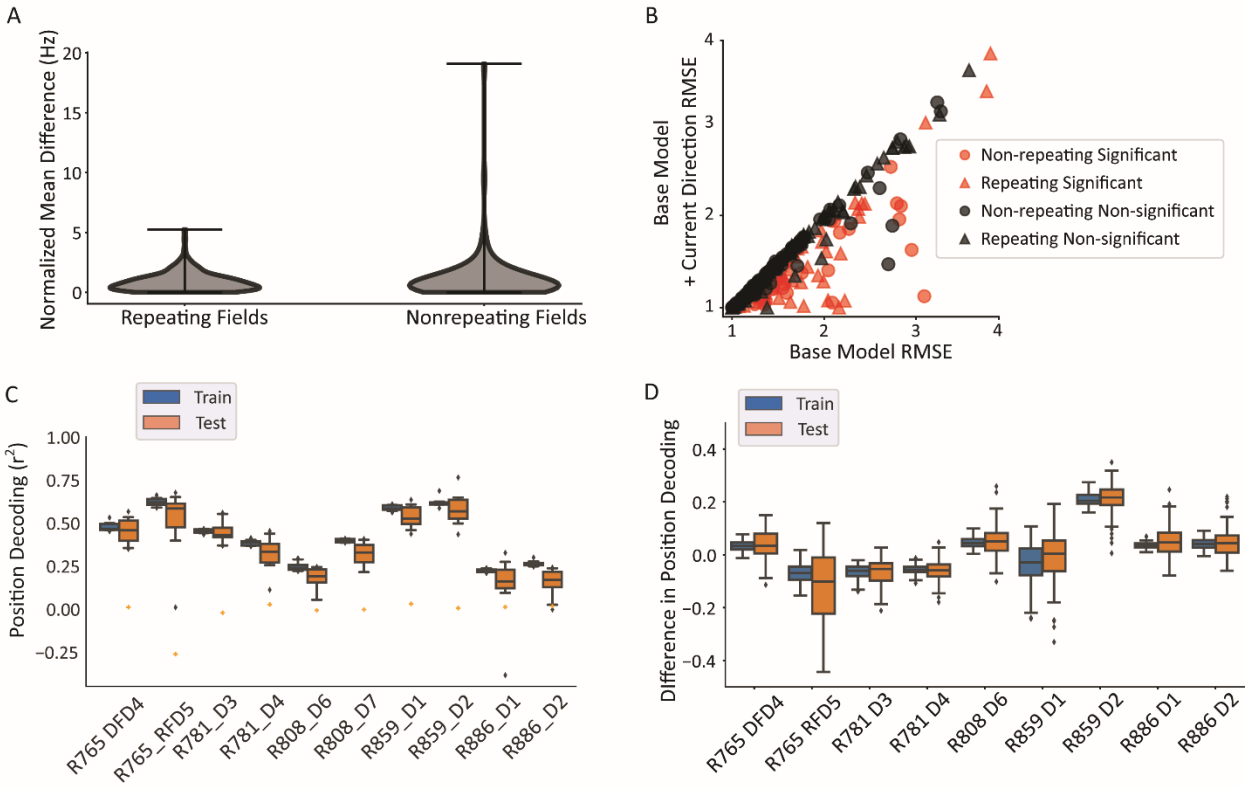

<u>Figure 4 – Repeating versus non-repeating fields directionality and spatial decoding.</u> **A.** The distribution of directional firing metrics for each repeating or non-repeating field. Directional firing was computed, as above, as the unsigned difference between the average firing rate in each of the two directions through the field. The two populations were not different from one another (repeating fields 0.88 ± 0.81 versus non-repeating fields 1.21 ± 1.97 normalized Hz; Mann-Whitney U = 11883, p = 0.49). **B.** GLM model comparison as in Fig 3C, separated by whether the field was repeating or not. There was no difference in either the proportion of fields that were significant in each category (69/172 repeating field portions vs. 51/125 field portions, $X^2(1) = 0.001$, p = 0.97) or the degree of improvement to the model fit (RMSE differences in base vs direction model, repeating = -0.104, non-repeating = -0.145, Mann Whitney U = 9764, p = 0.088). The same outlier was removed from visualization as in Fig 3C. **C.** Position decoding from training and testing data across datasets. Each box plot is the decoding performance (from training or test epochs) from 1000 rotations of the training/test window boundaries. Orange dot indicates the 95th percentile of a shuffled distribution formed by circularly shuffling the rat's position with respect to the neural population activity vector. The median decoder performance was 0.38 ± 0.29 (IQR). **D.** The difference in decoder performance from datasets in 4C using only repeating or nonrepeating neurons. The group with the smaller sample size was down-sampled 10 times per rotation of the train/test windows and the performance averaged. Nonrepeating performance was subtracted from repeating performance and the distribution of differences is shown for train and test sets. Most datasets had differences near 0, indicating that overall, there was little difference in decoding performance for repeating vs. nonrepeating cells.

maze. Relatedly, it is possible that days with poorer behavioral sampling (though still good enough to pass the sampling thresholds) led to poorer decoding as there were fewer samples to decode at undersampled locations.

Previous studies have shown that CA1 fields respond to future or previous directions along the present route (i.e., noncurrent directions) as well as the current direction, which has been interpreted as encoding the spatial decisions along a learned route (Ferbinteanu and Shapiro, 2003; Smith and Mizumori, 2007). The presence of retrospective or prospective coding was tested for each field. A GLM was used with regressors for current direction, previous direction, next direction, and, for the reasons mentioned above, time. The number of orientation-filtered fields with a significant effect of prospective or retrospective direction was not more than expected by chance by shuffling directional labels 1000 times and rerunning the GLM analysis. However, the effect of retrospective direction trended towards significance (Fig S4), indicating that there may be a possible weak effect of retrospective direction in the dataset.

Repeating versus Nonrepeating Fields

It has been hypothesized that repeating neurons have multiple fields because they are tuned to similar paths that are performed at each field location ("path equivalence", Frank et al., 2000; Singer et al., 2010). If this is the case, then one may expect repeating neurons to be more directional than nonrepeating neurons. However, the distributions of average normalized firing rate differences in each direction (analyzed as in Fig 3B) were not statistically different between repeating and nonrepeating neurons, with a mean difference of 0.88 normalized Hz for the repeating fields and 1.21 normalized Hz for the non-repeating fields (Mann-Whitney U = 11883, p = 0.49; Fig 4A). To corroborate this lack of difference, a GLM LRT test was used as before (Fig 4B). Here, too, there was no difference in the strength of tuning as assessed by differences in the root mean squared error (RMSE) between the base model and the current direction model, as the mean improvement in model fit was not significantly different between the groups (Mann-Whitney U = 9764, p = 0.088). Further, the proportions of directional fields were not different between the groups (69/172 repeating fields versus 51/125 non-repeating fields, Pearson's Chi-square $X^2(1) = 0.001$, p = 0.97). These data indicate that repeating fields were equally likely to be directionally tuned as non-repeating fields and those that were directional in each group had similar tuning strength.

The accuracy of position decoding from populations of repeating place cells is unclear given that their discharge is spatially ambiguous, yet fewer cells are needed to cover a given environment. A linear regression classifier was used to decode position from a population vector of neural firing rates. Spikes were convolved to yield a firing probability trace over time for each neuron. At each timepoint, the vector of the population activity of all cells (repeating and nonrepeating) was used to predict the x and y coordinates of the position, separately. The coefficient of determination (r^2) was used as the readout of decoder performance. Position could be reliably decoded from the population activity (median performance above 95th percentile of shuffled data in 10/10 datasets, binomial test $p = 9.76 \times 10^{-14}$; Fig. 4C). Repeating and nonrepeating cells were then analyzed separately. The difference in decoding performance between subpopulations of repeating and non-repeating neurons (with the larger group downsampled) shows that both groups of neurons were similarly informative about position (average difference = 0.06 ± 0.21, t-test compared to 0, t(8) = 0.923, p = 0.38; Fig 4D).

Nonconservation of Nonpositional Inputs across Repeating Fields

Place field repetition offers an opportunity to better understand how CA1 place cells integrate the positional inputs that determine their firing locations with the nonpositional inputs that modulate the firing rates in their fields. The OAS analysis in Figure 2D demonstrates that many neurons with multiple fields share a common input instructing them about what type of position to fire in – vertical or horizontal alleys. Because repeating fields share a common positional signal, they can serve as an internal control to test independently the contributions of the nonpositional signals. One possibility is that repeating fields share their directional tuning, that is, both the positional and nonpositional properties of a place field are repeated across the environment. Indeed, as stated above, it has been hypothesized that repetition reflects a common tuning among the fields to some path-related parameter (Frank et al., 2000). Alternatively, it is possible that at least some repeating neurons receive spatially gated directional inputs, and thus repeating fields from the same neuron may not always share a common directional tuning. Such a finding would suggest that the positional and nonpositional aspects of a place field's firing are dissociable.

To compare these alternative possibilities, the pattern of directional firing across repeating fields was tested. Fields within each repeating neuron were separated by orientation to equate the directions being compared. Directional tuning was not always conserved across repeating fields. For instance, neuron 1 of Fig 5A had four fields in horizontal alleys, three of which had sufficient sampling for analysis. Fields 0 and 2 fired more strongly for east over west while field 1 was untuned (two-way ANOVA interaction field x direction $F(2) = 5.32$, $p = 0.006$). Neuron 2 had two fields in vertical alleys with opposite tuning. Field 0 fired more strongly for south while field 1 did so for north (two-way ANOVA interaction field x direction $F(1) = 9.79$, $p = 0.0025$). To understand the distribution of directionality across repeating fields, a pairwise comparison was made between the directionality index of a given field and all other fields with the same orientation from the same cell and these comparisons were pooled across the population. The directionality index was calculated as the difference in the average firing rates between travel in either direction, normalized by both the mean firing of the field as well as location of each pass in the field. This distribution was centered at zero with density extending into all four quadrants, with a slight bias for fields to share the same tuning (113 pairs sharing, 81 not sharing directional tuning (Chi-square goodness of fit test $X^2(1) = 5.28$, $p = 0.022$; Fig 5B). The polarity explained very little of the variance in the data (OLS $r^2 = 0.045$, $p = 0.007$). Thus, although there was a slight trend for repeating fields to share the same directional bias, the size of the effect was small, demonstrating that repeating fields overall are weakly correlated in their directional tuning.

Given the role of borders and local topology on firing within the hippocampus and its inputs (O'Keefe and Burgess, 1996; Skaggs and McNaughton, 1998; Frank et al., 2000; Savelli et al., 2008, 2017; Liu et al., 2021), it was hypothesized that the geometry of the apparatus may influence the pattern of directional firing within repeating neurons. Field pairs were divided into whether the fields comprising the pair were on the same corridor or different corridors of the maze. Corridors were defined as the linearly concatenated alleys running the length or width of the track (Fig 5C, D bottom schematics) Field pairs from the same corridor had a significant positive correlation in their directional tuning (OLS $r^2 = 0.237$, $p = 0.00012$, Fig 5C). However, pairs on different corridors were not correlated with one another (OLS $r^2 = 0.017$, $p = 0.125$, Fig 5D). These correlations were significantly different from one another ($Z = 2.49$, $p = 0.0063$, one-

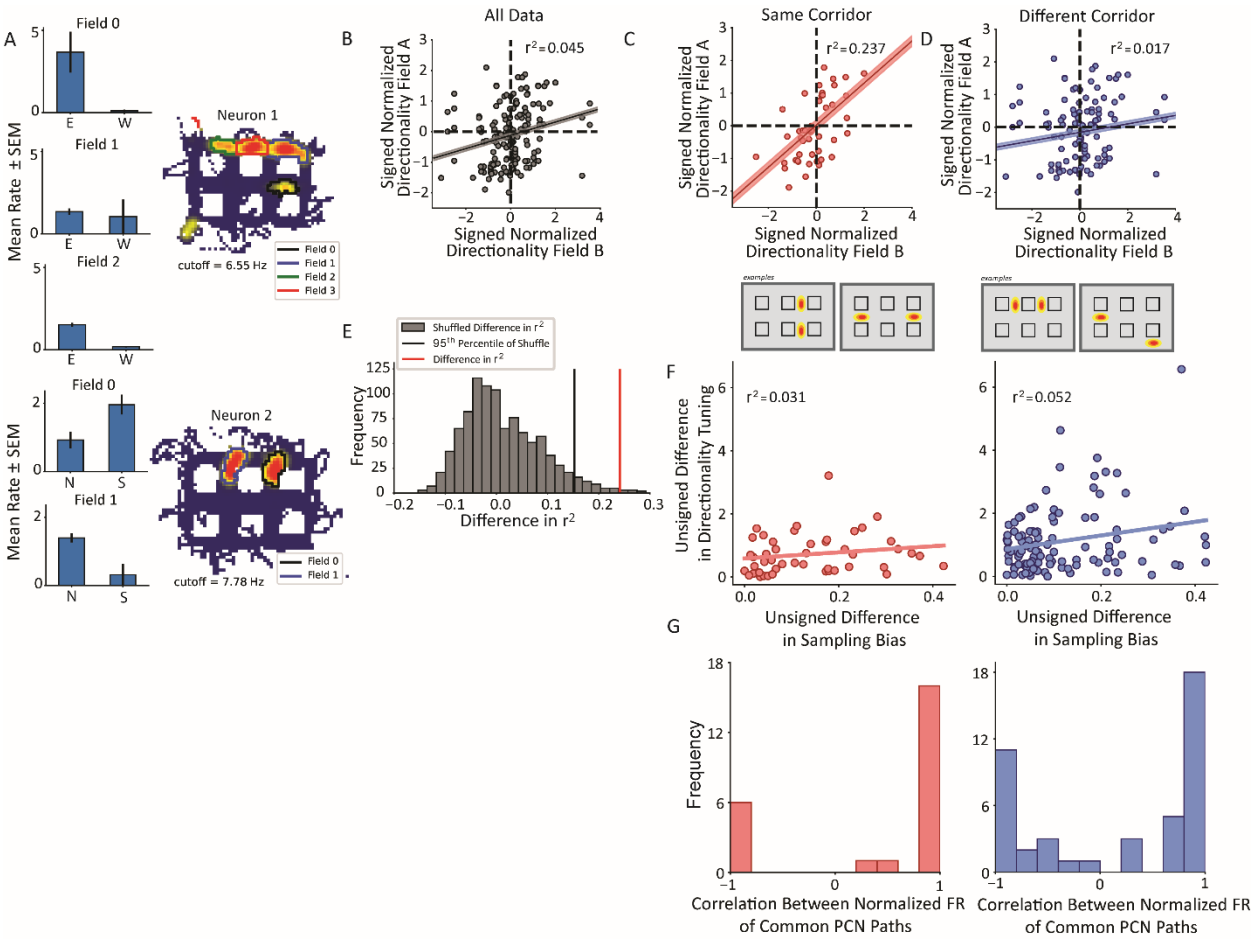

Figure 5 – Nonconservation of repeating field directionality. A. Examples of repeating neurons with directional tuning that was not conserved across fields. Top, neuron with four fields in horizontal alleys, three of which had sufficient sampling for analysis. Fields 0 and 2 preferred east over west while field 1 was untuned. Bottom, two fields primarily in vertical alleys that display opposite tuning patterns such that field 0 fires more strongly for south and field 1 for north. **B.** The pairwise correlation in directionality tuning between all pairs of aligned repeating fields within the same cell. The directionality index for each field was normalized by the field's maximum. The correlation between points explains little of their variance (r^2 = 0.045, p = 0.007). Pairs of fields were overall not much more likely to share (i.e., Quadrants I and III) as to not share (i.e., Quadrants II and IV) directional tuning. **C, D.** Field pairs were broken down based on whether the fields were on the same corridor or different corridors. Two examples of each type of relationship are shown (bottom schematics). North and east were taken as positive, by convention. Field pairs on the same kind of segment had a higher correlation (R^2 = 0.237, p = 0.00012) than those that were on different segments (R^2 = 0.017, p = 0.125). The difference between the correlations was significant using a Fischer's r-to-Z transformation (independent sample, one-sided test, z = 2.49, p = 0.0063). **E.** The difference in panels C-D was corroborated using a shuffling procedure. The labels for field pairs were shuffled while maintaining sample size. The difference $R^2_{same_shuffle} - R^2_{different_shuffle}$ was computed. The 95th percentile of this distribution was 0.155 which was less than the observed difference of 0.219. **F.** The pairwise comparison of sampling bias and directional tuning between fields on same or different corridors. The sampling bias explained little in the pattern of directionality differences between fields in either corridor group. **G.** Correlation between average response to each route shared by fields comprising pairs on same (red) or different (blue) corridors showed bimodal distributions. A Hartigan's test showed that the distributions were not unimodal.

sided independent sample Fisher's Z-transformation test). These data suggest that the weak positive correlation in the total population of pairs is explained by a stronger correlation among the same corridor field pairs alone. This effect was corroborated by a shuffling approach. Labels of each field pair were shuffled while preserving the sample size of the two groups (same corridor, different corridor). The difference in r^2 was computed on each iteration between the two groups and the distribution of such values was compared to the real difference in r^2 values. The real difference of 0.219 was greater than the 95th percentile of the null distribution of differences which was equal to 0.155 (Fig 5E).

The effect of corridor on repeating field directionality is unlikely to be explained by behavioral sampling. Figure 5F quantifies the correlation in directional sampling between field pairs on the same corridor versus different corridors. For each field, the directional sampling bias was computed as the ratio of the number of passes in the direction sampled more frequently to the total number of passes. The unsigned difference in the sampling biases of the fields was compared to the unsigned difference in the field's respective directionality tuning. Very little variance in the pairwise directionality comparison was attributable to the differences in sampling bias (same corridor $r^2 = 0.031$, $p = 0.23$; different corridor $r^2 = 0.052$, $p = 0.016$) suggesting that the observed results were not driven primarily by imbalanced sampling of preferred and anti-preferred directions of directionally tuned fields.

The distances between fields forming a pair on the same corridor (17.55 ± 7.56 bins) were similar to fields on different corridors (20.1 ± 8.27 bins), although the small difference was statistically significant (Mann Whitney U = 2097, $p = 0.031$; Fig S5A). This result suggests that a widely tuned spatial input is not the primary driver of the dissociation in directional correlations. The path taken to reach each field of a pair on the same corridor was shorter (4.17 ± 2.54 alleys) than between fields on a different corridor (8.01 ± 3.47 alleys) (Mann Whitney U = 607, $p = 8.04 \times 10^{-11}$; Fig S5B), raising the possibility that the routes between the fields systematically differed and this difference affected the shared directional tuning.

Last, we investigated whether a more specific analysis of routes would show a tendency for repeating cells to show route coding. Routes were defined as sequences of heading directions (previous, current, and next) through the fields (e.g., east-north-east, south-west-north, etc.) and each trajectory through a field was assigned to such a route. For each pair of commonly oriented fields, the correlation coefficient was calculated between the average responses to each type of route sampled through both fields. This analysis revealed a non-unimodal distribution (Hartigan's dip test statistic = 0.122, $p < 2.2 \times 10^{-16}$, corridor conditions pooled together; Fig 5G), with over half of all field pairs having a positive correlation (56% percent pairs correlation > 0.5). Therefore, although a majority of field pairs tended to share a pattern of route responses, a substantial fraction did not. Among the latter pairs, the responses were mostly anti-correlated (i.e., the correlations were close to –1). These data suggest that field pairs are affected by the route through the field, since they tended to respond to the same route – either by sharing their firing or having opposite responses. By contrast, very few field pairs were uncorrelated in their response to the same trajectory.

Time Dynamics of CA1 Firing Rates

CA1 activity patterns change across disparate timescales (Pastalkova et al., 2008; MacDonald et al., 2011; Manns et al, 2007) in ways that may support the encoding of temporal context (Ziv et al., 2013; Cai et al., 2016; Mankin et al, 2012). Prominent temporal non-stationarities were observed in the present study, taking on a number of different qualitative

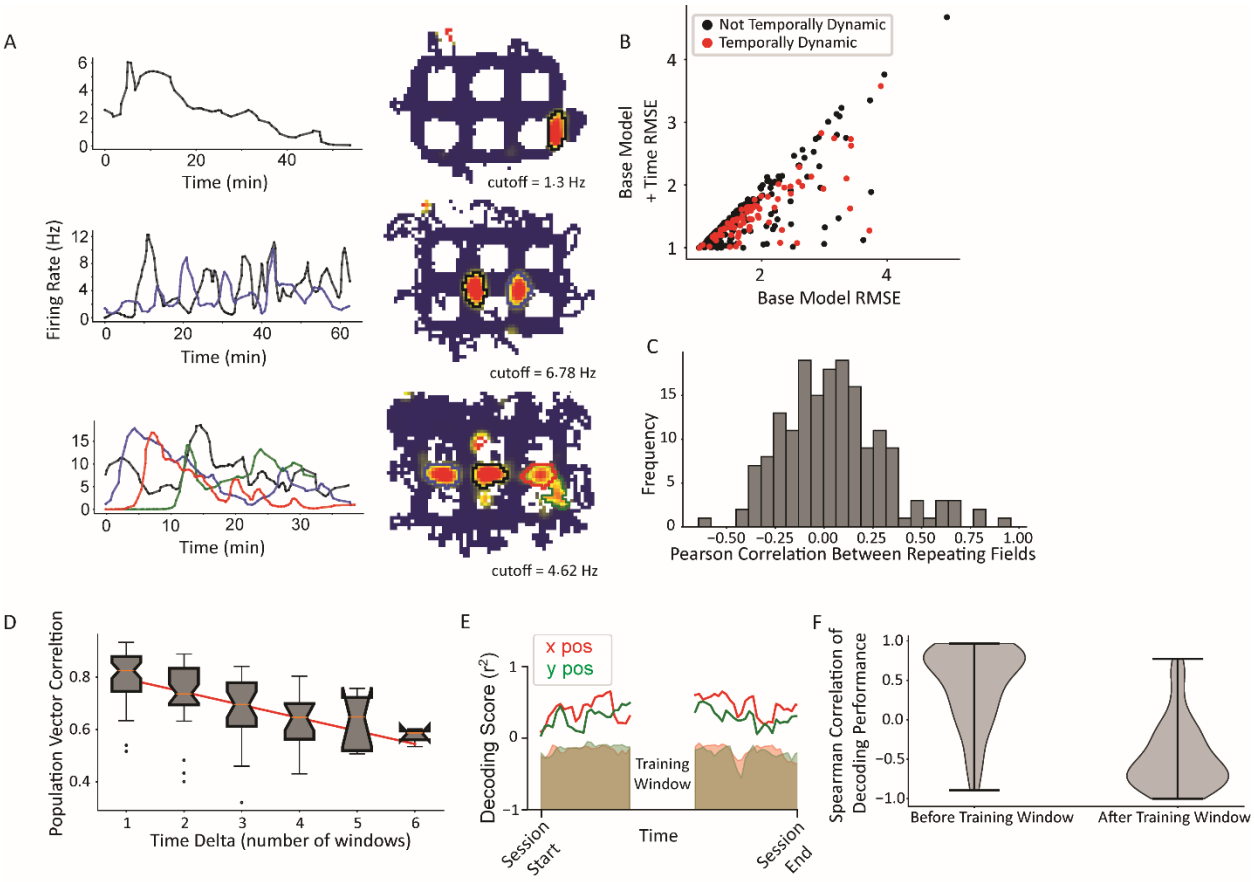

Figure 6 – Temporal dynamics. **A.** Examples of neurons with temporally dynamic place fields. Top, neuron with single field in a vertical alley. The field rate increases to a peak that is maintained for roughly ten minutes, before slowly decaying toward near silence over the rest of the session. Middle, repeating neuron with two fields in vertical alleys. The fields appear to have complex periodic dynamics over time. Further, they appear to be in an approximate anti-phase relationship in approximately the first half of the session, such that when the west field (black) is more active, the east field (blue) is at a local trough, and vice versa. Bottom, repeating cell with four fields, three of which are in horizontal alleys. Each field peaks with a different delay and then gradually decays over time. The delays are such that the times during which each field is active tile the whole session and the cell maintains its overall activity over time. **B.** A GLM likelihood ratio test to determine whether fields are temporally dynamic. The base model included current direction, for an analogous reason as to why time was included in the base model when testing for current direction. Time was represented as a natural spline with three degrees of freedom. A significant number of fields changed their firing rates over time (83/296 field pieces, $p = 2.07 \times 10^{-38}$, alpha = 0.0083 for three spline knots multiplied by (up to) two orientations per field). **C.** Pairwise comparisons of the firing rate time series of pairs of repeating fields were computed using Pearson's correlation. The firing rate time series were interpolated to equate their sample sizes using a PCHIP interpolation. The distribution was centered near zero with a wide distribution (mean = 0.049 ± 0.26). **D.** Pairwise correlations between activity patterns in different time windows. Time windows closer together are more correlated than those further away. There was no significant difference in the slope of the decorrelation between repeating and nonrepeating neurons (Fig. S6). **E.** Example time window from single dataset showing portion of data held out for training (white space, center) and the decoding performance on the rest of the data divided into temporal windows. Shaded region is shuffle. Red corresponds to x position data, green to y position data. **F.** Distribution of Spearman correlation of decoding performance before or after the training window shows the gradual decrease in decoder performance with increasing distance from the training window.

patterns (Fig 6A). Figure 6A (top) shows an example of a single-field cell that decreased its firing rate over the course of the session. Other cells (not shown) increased their firing rates over the session. Intriguingly, repeating fields of the same cell also showed temporal dynamics that were decoupled in time. Figure 6A (middle) shows a cell with two repeating fields that showed antiphase temporal dynamics for the first 40 min (i.e., the firing rates of each field

waxed and waned out of phase with each other). Figure 6A (bottom) shows a final example of a repeating cell with 4 fields (3 horizontal and 1 vertical) that each showed a rapid increase in firing rate followed by a slow decline, but the temporal onset varied across the fields.

Across all cells, a GLM approach identified a significant number of fields that exhibited significant time dynamics (83/296 oriented fields; binomial test, $p = 2.07 \times 10^{-38}$; average increase in fit 0.26 ± 0.38; Fig 6B). Repeating and nonrepeating fields were equally likely to exhibit temporal dynamics, demonstrating a similar lack of difference seen in directional tuning (66/171 repeating fields, 39/125 non-repeating fields, Pearson's Chi-square $X^2(1) = 0.53$, $p = 0.42$). Fields from the same repeating neuron were also analyzed to see if their time dynamics were correlated. The Pearson correlation between the firing rate time series was computed between each pair of fields of each repeating neuron (Fig 6C). This distribution was centered at zero, suggesting fields were not more likely to be correlated or anti-correlated with one another (mean correlation = 0.049 ± 0.26).

These time dynamics resulted in gradual changes in the population activity over time. Data from each recording day were split into 6 windows and the population vector correlations between windows were calculated. More distant windows were less correlated (average slope per data set –0.06 ± 0.022, two-sided t-test compared to 0, $t(9) = 7.88$, $p = 2.49 \times 10^{-5}$; Fig 6D), consistent with prior work (Manns et al., 2007; Mankin et al., 2012). This trend was maintained within both repeating and nonrepeating groups separately (Fig S6). To explicitly test the change in positional information over time, a sliding window was moved across the session and the data in each window was used to train a linear regression classifier. The data in the training window was tested on all other windows (Fig 6E). This analysis revealed that the decoding performance was high near the training window and decayed outside of it, yielding a positive slope (mean Spearman correlation = 0.44 ± 0.49, one-sided t-test (greater), $t = 7.59$, $p = 5.11 \times 10^{-11}$) to the performance in the window before the training window and a negative slope (mean Spearman correlation = -0.45 ± 0.43, one-sided t-test (less), $t = 10.0$, $p = 1.53 \times 10^{-16}$) to the performance after the training window (Fig 6F). Together, these data are consistent with previous work showing that time dynamics within CA1 are graded at the population level (Manns et al., 2007; Mankin et al., 2012), which is theoretically capable of providing a temporal context signal (Ziv et al., 2013; Cai et al., 2016, Tsao et al., 2018).

Discussion

Analyzing the heading direction through place fields, both repeating and non-repeating, provided insight into three topics of CA1 physiology and its potential relationship to episodic memory formation according to O'Keefe and Nadel's (1978) cognitive map theory. First, the presence of directional firing on a maze that had properties of both random foraging and directed navigation tasks suggested that the low degrees-of-freedom for path choices resulted in the system distinguishing between the paths, possibly because they differed from one another in limited ways constrained by the geometry of the apparatus rather than continuously, as they would on an open platform. Second, comparing directional tuning across repeating fields revealed a distinction between positional inputs (i.e., inputs that tell a place cell *where* to fire) and nonpositional inputs (i.e., inputs, including spatial inputs, that tell a place cell *how strongly* to fire in its place field). Last, in spite of the spatial ambiguity introduced by multifieldedness and temporal dynamics, the map maintained a stable spatial signal but exhibited gradual temporal dynamics, with repeating fields showing temporally dissociable changes similar to their dissociation in directionality.

Directionality, Route Coding, and Place Field Repetition

Place fields are more directional when animals perform directed, stereotyped trajectories on unidimensional tracks (McNaughton et al 1983; Markus et al. 1995; Liberti et al., 2022) compared to 2-dimensional foraging in an open field (Muller et al., 1994; Markus et al., 1995; but see Rubin et al., 2014; Acharya et al., 2016). The city-block maze of the present study had aspects of both types of behavior, as the rats could move in 2 dimensions, but their trajectories were constrained to a rectilinear grid. Nonetheless, many place cells showed strong directionality and, furthermore, showed large numbers of repeating fields. This combination of place field repetition and directionality has been interpreted as evidence for route encoding, or "path equivalence," in which spatially selective neurons in the hippocampus or entorhinal cortex fire in similar locations along a trajectory that is repeated at different locations in an environment. The data presented here suggest that route encoding by repeating fields is likely to be more complex than previously characterized (Frank et al., 2000; Singer et al., 2010). In the previous work, route coding was explored on apparatuses with a constrained set of choices (Frank et al., 2000; Singer et al., 2010; Grieves et al., 2016b; Ferbinteanu and Shapiro, 2007; Smith and Mizumori, 2007; Wood et al., 2000). These studies found neurons tuned to different types of turns and they suggested that more complex routes might be encoded on apparatuses where such routes could be sampled. The present work utilized such an apparatus and provided qualified support for this suggestion. Due to the unstructured nature of the task, the data lacked the power to test whether any particular complex route (defined as a sequence of headings into, through, and out of an alley) was encoded by individual neurons. Thus, current direction alone was used as a simple proxy for the potentially complex path through the field. If place-field repetition reflected the hippocampus encoding equivalent paths in an environment, then the different fields of a repeating cell should show the same current direction preference. Although previous work has demonstrated a role for heading in gating the presence of repetition (Grieves et al., 2016a; Harland et al., 2017; Cowen and Nitz, 2014, Derdikman et al., 2009), it remained unclear if a common representation of heading was the input driving repeating fields. In the present work, many repeating fields were uncorrelated in their responses to heading (at least when the repeating fields were on different corridors), showing that directional preference *per se* was not the driving force underlying repetition under the conditions of the present study.

Although the lack of shared directional preference in many neurons suggested that these neurons were not encoding routes in a simple manner, we nonetheless observed that the repeating fields of many cells showed strong correlations in their firing rates across the different types of complex trajectories through the fields (i.e., previous, current, and next alleys) (Fig 5G). This result suggested that a subset of repeating fields may indeed encode route. However, many repeating fields in different corridors were uncorrelated or anticorrelated in their route responses. Thus, place field repetition may result from multiple mechanisms that give rise to similar phenomena: a subset of repeating fields may encode route while another subset encodes a different dimension, such as local border geometry.

The potential contribution of local border geometry to place field repetition is supported by multiple studies and was specifically proposed as a mechanism in one modeling study (Grieves et al., 2017). In the present work, as well as others recording from multiple compartments (Skaggs and McNaughton, 1998; Spiers et al., 2015; Grieves et al., 2016), the local border geometry was shared across fields of multi-fielded neurons (Fig 2D). Cells in the present work were disproportionately likely to have fields with borders on the same sides of the field, i.e. to be aligned along an axis of the maze (vertical or horizontal) (this is similar to axis-tuned cells reported by Olson et al., 2017). In previous work, fields occurred in the same relative position in multiple adjacent boxes (Skaggs and McNaughton, 1998; Spiers et al., 2015; Grieves et al., 2016). This hypothesis is consistent with the inputs that CA1 receives. Boundary vector

cells (Lever et al., 2009, Stewart et al., 2014) and border cells (Barry et al., 2006; Savelli et al., 2008; Solstad et al., 2008) exist within the circuitry of the hippocampal formation and it is known that CA1 neurons are modulated by changes to the local border configuration (O'Keefe and Burgess, 1996). Thus, it is plausible that repetition may be caused by stronger border-related input to these neurons. The paths available at a location are partially determined by the configuration of borders, therefore the hypotheses discussed above are related. Future work would require the dissociation of the pattern of borders and the types of paths available to the animal at each location to disentangle the effect of these variables.

Leveraging Repetition to Understand Positional vs Nonpositional Inputs

Place field repetition offers a unique opportunity to explore how inputs are functionally organized in CA1. According to the cognitive map theory (O'Keefe and Nadel, 1978), the hippocampus leverages the spatial framework of the place map to bind together different aspects of an experience into a coherent representation in support of episodic memory storage and retrieval. The present data provide evidence that this process is assisted by individual field addressability, wherein different nonpositional inputs (i.e., experiential inputs) affect a neuron's response differently at different fields.

The rate remapping hypothesis stipulates a mechanism to encode nonpositional inputs – such as changes to the sensory features of an environment or differences in how the animal navigates through the environment – through changes to the pattern of firing rates across spatially stable place fields (Leutgeb et al., 2005; Shapiro and Eichenbaum, 1997). This rate remapping allows for flexible encoding of the episodic content of experience while maintaining a stable map. Such episodic content may include nonspatial variables, such as alterations in objects or the wall colors of an environment, or spatial variables that are related to navigation but do not define specific positions. For example, direction and speed can alter the firing rates of place cells (McNaughton et al., 1983; Markus et al., 1995; Czurkó et al., 1999; Maurer et al., 2012; Huxter et al., 2003), and fields of "splitter cells" can alter their firing rates depending on the upcoming (or previous) spatial choice, while the field locations remain mostly stable (Wood et al., 1999; Frank et al., 2000; Ferbinteau and Shapiro, 2003). These results suggest that inputs that are spatial but do not explicitly encode position may be encoded similarly as purely nonspatial inputs such as odors or sounds. Thus, we have used the term nonpositional (as opposed to nonspatial) to denote how various cues can alter the firing rates of place cells while maintaining the positional specificity of the place field intact.

Repeating place fields provided a within-cell control to demonstrate that positional inputs (e.g., inputs that tell a place field where to fire) and nonpositional inputs (i.e., inputs that tell the neuron how strongly to fire in its field) are organized differently in CA1. The simplest model would suggest that both sets of inputs are fixed for each place cell. Thus, the positional inputs would cause a cell to fire at similar locations in the environment (e.g., locations that share common elements of a trajectory or that share common geometric borders) and share the same nonpositional coding (e.g., similar direction preferences). However, such inflexibility would not be ideal for the hypothesized role of firing rate as encoding the episodic inputs onto a place field, which would require flexibility in encoding unpredictable experiential inputs at different locations. The present data utilize repeating fields to suggest that, within an environment, the positional inputs are relatively rigid, whereas the nonpositional inputs are more flexible, allowing different repeating fields to show different directional preferences. In other words, fields are individually addressable with respect to the nonpositional inputs they receive; they do not inherit their nonpositional tuning as a global property of the cell.

In different environments, the firing locations of place fields change when the system undergoes global remapping. This well-studied property suggests that the positional inputs can

also be dynamically gated and flexible between environments, even if they are more rigid within an environment. On the other hand, it is possible that the positional inputs are also rigid between environments, even as the place fields express different firing fields. For example, the boundary vector cell (BVC) model (O'Keefe and Burgess, 1996) postulates that each place cell receives input from a fixed set of BVCs that determine whether and where a cell will fire in an environment. In this model, a place field will be active if there is a location in the environment that drives each of its BVCs. Thus, it is the environmental geometry that determines whether a cell will show global remapping between environments, not flexible changes to its positional inputs (Hartley et al., 2000). Regardless of whether the positional inputs are rigid or flexible across environments, the present data suggest that the nonpositional inputs are always flexible, as expected if they encode the episodic content of an experience on a stable spatial framework.

The corridor analysis (Fig 5C,D) revealed that under certain conditions the nonpositional input tended to be shared across repeating fields, suggesting that experience may shape directional tuning. The difference in pairwise directional tuning between fields on the same and different corridors further emphasizes that fields were separately addressable in how they were tuned for direction. The difference in corridor was also correlated with behavioral biases in how animals sampled fields. Fields on the same corridor were usually sampled by shorter paths (Fig S5b) that did not necessarily involve a change in heading. However, traveling between fields on different corridors necessarily involved a change in heading and these paths were usually longer as well (Fig S5b). One explanation for these data is that fields sampled along contiguous routes, without interruptions from heading change or reward delivery, are more likely to share their directionality. Directionality is affected by an animal's experience through the field (Navratilova et al., 2012), so it is possible the difference in experience between sampling fields on the same versus different corridors affects the directional tuning properties between them. Sequence learning mechanisms, such as theta phase precession or theta-gamma coding (Skaggs et al., 1996; Lisman et al., 2005; Terada et al., 2017) may also play a role. It is known that theta look-ahead sequences, in which non-local place field activity sweeps ahead of the animal, segment behavior by preferentially occurring at landmarks (Wikenheiser et al., 2015; Gupta et al., 2012). In the present study, turns at the ends of corridors, along with reward deliveries, may be salient task boundaries at which point theta sequences are terminated. Fields active within the same theta sequence (typically same corridor fields) may be functionally coupled, while fields active on opposite sides of a theta sequence termination (different corridor fields) may be uncoupled and their tuning uncorrelated.

Temporal Dynamics and Map Stability

The present data demonstrate a constant, gradual drift in the population activity pattern as the animal forages without a task. This affects the stability of the map over time; although the map maintains spatial informativeness at each point in time, the activity of the neurons comprising the map exhibit strong temporal non-stationarities. The time dynamics within individual repeating fields were heterogeneous and uncorrelated. This provides evidence for another nonpositional input, time, that is not conserved across fields. Previous studies have shown temporal drift hypothesized to serve as a temporal context signal to distinguish similar, repeated events (Manns et al., 2007; Ziv et al., 2013; Mankin et al., 2012). However, these studies did not show a constantly drifting signal in the absence of an explicit task, which would be predicted if these dynamics served as a temporal context signal. In one study examining temporal drift during a foraging task, only two short-term timepoints were used which made it difficult to determine whether there was a continuous signal (Mankin et al., 2012). In another study (Manns et al., 2007), drift was analyzed over shorter periods, but during an odor discrimination task which may recruit additional circuits than what would be used during free navigation. Therefore, the present data show that CA1 activity patterns are constantly drifting

even in the absence of a task (as demonstrated previously in LEC; Tsao et al., 2018) but in a way that preserves the spatial informativeness of the map.

The uncorrelated time dynamics within repeating fields provides further evidence that place cells do not receive a global gain signal that affects all fields equally. Fields changed at different times (Fig 6A) and at the population level this resulted in decorrelated repeating field time series (Fig 6B). It is important to note that because a Pearson correlation was used, it is possible the fields are related in time with a phase shift, and we did not have the statistical power to test this possibility adequately. Thus, although it is clear that the place fields of repeating cells do not change their firing rates in synchrony, as if the cell had a global excitability change that made all its fields wax and wane together, it nonetheless remains an open question as to whether the subfields of repeating cells engage in certain types of competitive interactions or other network dynamics that couple changes in their firing rates in more complex ways.

Random Foraging Versus Directed Navigation

The behavioral sampling of an environment may affect how the CA1 place map represents it. CA1 place cells distinguish between different behaviors as the animal traverses a field if those behaviors are relevant for goal-directed navigation. When rats were trained to run down the stem of a T-maze before making a choice, some neurons on the center stem common to both choices distinguished between the behaviors (Wood et al., 2000). These cells, termed “splitter cells”, have been recorded under a variety of circumstances (Ferbinteanu et al., 2003; Smith and Mizumori, 2006; Bower et al., 2005; Griffin et al, 2007; Grieves et al., 2016b, though see Lenck-Santini 2001). Common to these directed navigation experiments were stereotyped behaviors the animal learned, typically routes from a starting position to a goal. Place fields can also be directional, with their firing rates changing as a function of the direction of travel through the field (McNaughton et al., 1983; Wiener et al., 1989; Markus et al., 1995). Although it is possible directionality is caused by other correlates of direction change, e.g. changes in spatial view (McNaughton et al., 1991), another interpretation is that directionality and splitting both reflect common, or at least similar, mechanisms that cause place fields to fire differentially depending on the path through the field. For example, place fields became directional when animals were trained to run on an open platform in a stereotyped manner (Markus et al, 1995), conditions that are similar to those that elicit splitting and result in a qualitatively similar phenomenon. The conditions under which splitting/directionality are observed are not well understood and the presence of directionality shown here suggests that the pattern of behavioral sampling *per se* might be sufficient to cause splitting/directionality. The present design is a hybrid between the open foraging conditions, in which little directionality/splitting are seen, and the directed navigation tasks, in which splitting is observed. There were no specific paths for the animal to learn; it could freely navigate throughout the city-block maze. However, its behavior was constrained by the linear nature of each alley and the right-angle choice points. This resulted in a low choice degree-of-freedom on the maze. The fact that a substantial number of place fields distinguished between the directions of travel through their firing rates suggests that even without learned routes to perform, CA1 represented attributes of the path through the field. It is possible that the rat performed internally generated routes, and these were represented by CA1. Alternatively, the low choice degrees-of-freedom itself could have promoted the representation of route-related variables, possibly because of the discrete nature of travel through the maze. Regardless, these data demonstrate that explicit learning itself is not necessary for the hippocampus to represent how the animal moves through a maze.

References

Acharya, L., Aghajan, Z. M., Vuong, C., Moore, J. J., & Mehta, M. R. (2016). Causal Influence of Visual Cues on Hippocampal Directional Selectivity. *Cell*, *164*(1–2), 197–207. https://doi.org/10.1016/j.cell.2015.12.015

Alexander, A. S., & Nitz, D. A. (2017). Spatially Periodic Activation Patterns of Retrosplenial Cortex Encode Route Sub-spaces and Distance Traveled. *Current Biology*, *27*(11), 1551-1560.e4. https://doi.org/10.1016/j.cub.2017.04.036

Allen, T. A., Salz, D. M., McKenzie, S., & Fortin, N. J. (2016). Nonspatial Sequence Coding in CA1 Neurons. *The Journal of Neuroscience*, *36*(5), 1547–1563. https://doi.org/10.1523/JNEUROSCI.2874-15.2016

Anderson, M. I., & Jeffery, K. J. (2003). Heterogeneous Modulation of Place Cell Firing by Changes in Context. *The Journal of Neuroscience*, *23*(26), 8827–8835. https://doi.org/10.1523/JNEUROSCI.23-26-08827.2003

Aronov, D., Nevers, R., & Tank, D. W. (2017). Mapping of a non-spatial dimension by the hippocampal–entorhinal circuit. *Nature*, *543*(7647), 719–722. https://doi.org/10.1038/nature21692

Barry, C., Lever, C., Hayman, R., Hartley, T., Burton, S., O'Keefe, J., Jeffery, K., & Burgess, N. (2006). The Boundary Vector Cell Model of Place Cell Firing and Spatial Memory. *Reviews in the Neurosciences*, *17*(1–2), 71–97. https://doi.org/10.1515/REVNEURO.2006.17.1-2.71

Bower, M. R. (2005). Sequential-Context-Dependent Hippocampal Activity Is Not Necessary to Learn Sequences with Repeated Elements. *Journal of Neuroscience*, *25*(6), 1313–1323. https://doi.org/10.1523/JNEUROSCI.2901-04.2005

Breiman, L. (2001). Random Forests. *Machine Learning*, *45*(1), 5–32. https://doi.org/10.1023/A:1010933404324

Cai, D. J., Aharoni, D., Shuman, T., Shobe, J., Biane, J., Song, W., Wei, B., Veshkini, M., La-Vu, M., Lou, J., Flores, S. E., Kim, I., Sano, Y., Zhou, M., Baumgaertel, K., Lavi, A., Kamata, M., Tuszynski, M., Mayford, M., … Silva, A. J. (2016). A shared neural ensemble links distinct contextual memories encoded close in time. *Nature*, *534*(7605), 115–118. https://doi.org/10.1038/nature17955

Cowen, S. L., & Nitz, D. A. (2014). Repeating Firing Fields of CA1 Neurons Shift Forward in Response to Increasing Angular Velocity. *Journal of Neuroscience*, *34*(1), 232–241. https://doi.org/10.1523/JNEUROSCI.1199-13.2014

Czurkó, A., Hirase, H., Csicsvari, J., & Buzsáki, G. (1999). Sustained activation of hippocampal pyramidal cells by 'space clamping' in a running wheel: Sustained discharge of hippocampal pyramidal cells. *European Journal of Neuroscience*, *11*(1), 344–352. https://doi.org/10.1046/j.1460-9568.1999.00446.x

D. M. Smith, & Mizumori, S. J. Y. (2006). Learning-Related Development of Context-Specific Neuronal Responses to Places and Events: The Hippocampal Role in Context Processing. *Journal of Neuroscience*, *26*(12), 3154–3163. https://doi.org/10.1523/JNEUROSCI.3234-05.2006

Derdikman, D., Whitlock, J. R., Tsao, A., Fyhn, M., Hafting, T., Moser, M.-B., & Moser, E. I. (2009). Fragmentation of grid cell maps in a multicompartment environment. *Nature Neuroscience*, *12*(10), 1325–1332. https://doi.org/10.1038/nn.2396

Diedenhofen, B., & Musch, J. (2015). cocor: A Comprehensive Solution for the Statistical Comparison of Correlations. *PLoS ONE*, *10*(4), e0121945. https://doi.org/10.1371/journal.pone.0121945

Ferbinteanu, J., & Shapiro, M. L. (2003). Prospective and Retrospective Memory Coding in the Hippocampus. *Neuron*, *40*(6), 1227–1239. https://doi.org/10.1016/S0896-6273(03)00752-9

Fisher, R. A. (1921). On the 'probable error' of a coefficient of correlation deduced from a small sample. *Metron*, *1*, 1–32.
Frank, L. M., Brown, E. N., & Wilson, M. (2000). Trajectory Encoding in the Hippocampus and Entorhinal Cortex. *Neuron*, *27*(1), 169–178. https://doi.org/10.1016/S0896-6273(00)00018-0
Fritsch, F. N., & Butland, J. (1984). A Method for Constructing Local Monotone Piecewise Cubic Interpolants. *SIAM Journal on Scientific and Statistical Computing*, *5*(2), 300–304. https://doi.org/10.1137/0905021
Grieves, R. M., Jenkins, B. W., Harland, B. C., Wood, E. R., & Dudchenko, P. A. (2016). Place field repetition and spatial learning in a multicompartment environment. *Hippocampus*, *26*(1), 118–134. https://doi.org/10.1002/hipo.22496
Grieves, R. M., Wood, E. R., & Dudchenko, P. A. (2016). Place cells on a maze encode routes rather than destinations. *ELife*, *5*. https://doi.org/10.7554/eLife.15986
Grieves, R. M., Duvelle, É., Wood, E. R., & Dudchenko, P. A. (2017). Field repetition and local mapping in the hippocampus and the medial entorhinal cortex. *Journal of Neurophysiology*, *118*(4), 2378–2388. https://doi.org/10.1152/jn.00933.2016
Griffin, A. L., Eichenbaum, H., & Hasselmo, M. E. (2007). Spatial Representations of Hippocampal CA1 Neurons Are Modulated by Behavioral Context in a Hippocampus-Dependent Memory Task. *Journal of Neuroscience*, *27*(9), 2416–2423. https://doi.org/10.1523/JNEUROSCI.4083-06.2007
Hafting, T., Fyhn, M., Molden, S., Moser, M.-B., & Moser, E. I. (2005). Microstructure of a spatial map in the entorhinal cortex. *Nature*, *436*(7052), 801–806. https://doi.org/10.1038/nature03721
Harland, B., Contreras, M., Souder, M., & Fellous, J.-M. (2021). Dorsal CA1 hippocampal place cells form a multi-scale representation of megaspace. *Current Biology*, *31*(10), 2178-2190.e6. https://doi.org/10.1016/j.cub.2021.03.003
Harland, B., Grieves, R. M., Bett, D., Stentiford, R., Wood, E. R., & Dudchenko, P. A. (2017). Lesions of the Head Direction Cell System Increase Hippocampal Place Field Repetition. *Current Biology*, *27*(17), 2706-2712.e2. https://doi.org/10.1016/j.cub.2017.07.071
Harris, C. R., Millman, K. J., van der Walt, S. J., Gommers, R., Virtanen, P., Cournapeau, D., Wieser, E., Taylor, J., Berg, S., Smith, N. J., Kern, R., Picus, M., Hoyer, S., van Kerkwijk, M. H., Brett, M., Haldane, A., del Río, J. F., Wiebe, M., Peterson, P., … Oliphant, T. E. (2020). Array programming with NumPy. *Nature*, *585*(7825), 357–362. https://doi.org/10.1038/s41586-020-2649-2
Hartley, T., Burgess, N., Lever, C., Cacucci, F., & O'Keefe, J. (2000). Modeling place fields in terms of the cortical inputs to the hippocampus. *Hippocampus*, *10*(4), 369–379. https://doi.org/10.1002/1098-1063(2000)10:4<369::AID-HIPO3>3.0.CO;2-0
Hayman, R., Verriotis, M. A., Jovalekic, A., Fenton, A. A., & Jeffery, K. J. (2011). Anisotropic encoding of three-dimensional space by place cells and grid cells. *Nature Neuroscience*, *14*(9), 1182–1188. https://doi.org/10.1038/nn.2892
Herzog, L. E., Katz, D. B., & Jadhav, S. P. (2020). Refinement and Reactivation of a Taste-Responsive Hippocampal Network. *Current Biology*, *30*(7), 1306-1311.e4. https://doi.org/10.1016/j.cub.2020.01.063
Herzog, L. E., Pascual, L. M., Scott, S. J., Mathieson, E. R., Katz, D. B., & Jadhav, S. P. (2019). Interaction of Taste and Place Coding in the Hippocampus. *The Journal of Neuroscience*, *39*(16), 3057–3069. https://doi.org/10.1523/JNEUROSCI.2478-18.2019
Hunter, J. D. (2007). Matplotlib: A 2D Graphics Environment. *Computing in Science & Engineering*, *9*(3), 90–95. https://doi.org/10.1109/MCSE.2007.55
Huxter, J., Burgess, N., & O'Keefe, J. (2003). Independent rate and temporal coding in hippocampal pyramidal cells. *Nature*, *425*(6960), 828–832. https://doi.org/10.1038/nature02058
Itskov, P. M., Vinnik, E., & Diamond, M. E. (2011). Hippocampal Representation of Touch-Guided Behavior in Rats: Persistent and Independent Traces of Stimulus and Reward Location. *PLoS ONE*, *6*(1), e16462. https://doi.org/10.1371/journal.pone.0016462

Ji, D., & Wilson, M. A. (2008). Firing Rate Dynamics in the Hippocampus Induced by Trajectory Learning. *Journal of Neuroscience*, *28*(18), 4679–4689. https://doi.org/10.1523/JNEUROSCI.4597-07.2008

Komorowski, R. W., Manns, J. R., & Eichenbaum, H. (2009). Robust Conjunctive Item-Place Coding by Hippocampal Neurons Parallels Learning What Happens Where. *Journal of Neuroscience*, *29*(31), 9918–9929. https://doi.org/10.1523/JNEUROSCI.1378-09.2009

Lee, J. S., Briguglio, J. J., Cohen, J. D., Romani, S., & Lee, A. K. (2020). The Statistical Structure of the Hippocampal Code for Space as a Function of Time, Context, and Value. *Cell*, *183*(3), 620-635.e22. https://doi.org/10.1016/j.cell.2020.09.024

Lenck-Santini, P.-P., Save, E., & Poucet, B. (2001). Place-cell firing does not depend on the direction of turn in a Y-maze alternation task: Place cells and memory. *European Journal of Neuroscience*, *13*(5), 1055–1058. https://doi.org/10.1046/j.0953-816x.2001.01481.x

Lenth, R. (2020). *emmeans: Estimated Marginal Means, aka Least-Squares Means*. https://CRAN.R-project.org/package=emmeans

Leutgeb, S. (2005). Independent Codes for Spatial and Episodic Memory in Hippocampal Neuronal Ensembles. *Science*, *309*(5734), 619–623. https://doi.org/10.1126/science.1114037

Lever, C., Burton, S., Jeewajee, A., O'Keefe, J., & Burgess, N. (2009). Boundary Vector Cells in the Subiculum of the Hippocampal Formation. *Journal of Neuroscience*, *29*(31), 9771–9777. https://doi.org/10.1523/JNEUROSCI.1319-09.2009

Liberti, W. A., Schmid, T. A., Forli, A., Snyder, M., & Yartsev, M. M. (2022). A stable hippocampal code in freely flying bats. *Nature*. https://doi.org/10.1038/s41586-022-04560-0

Liu, K., Sibille, J., & Dragoi, G. (2021). Orientation selectivity enhances context generalization and generative predictive coding in the hippocampus. *Neuron*, *109*, 1–11. https://doi.org/10.1016/j.neuron.2021.08.013

MacDonald, C. J., Lepage, K. Q., Eden, U. T., & Eichenbaum, H. (2011). Hippocampal ``Time Cells'' Bridge the Gap in Memory for Discontiguous Events | Elsevier Enhanced Reader. *Neuron*, *71*, 737–749. https://doi.org/10.1016/j.neuron.2011.07.012

Maechler, M. (2021). *Diptest: Hartigan's Dip Test Statistic for Unimodality—Corrected*. https://CRAN.R-project.org/package=diptest

Mankin, E. A., Sparks, F. T., Slayyeh, B., Sutherland, R. J., Leutgeb, S., & Leutgeb, J. K. (2012). Neuronal code for extended time in the hippocampus. *Proceedings of the National Academy of Sciences*, *109*(47), 19462–19467. https://doi.org/10.1073/pnas.1214107109

Manns, J. R., & Eichenbaum, H. (2009). A cognitive map for object memory in the hippocampus. *Learning & Memory*, *16*(10), 616–624. https://doi.org/10.1101/lm.1484509

Manns, J. R., Howard, M. W., & Eichenbaum, H. (2007). Gradual Changes in Hippocampal Activity Support Remembering the Order of Events. *Neuron*, *56*(3), 530–540. https://doi.org/10.1016/j.neuron.2007.08.017

Markus, E., Qin, Y., Leonard, B., Skaggs, W., McNaughton, B., & Barnes, C. (1995). Interactions between location and task affect the spatial and directional firing of hippocampal neurons. *The Journal of Neuroscience*, *15*(11), 7079–7094. https://doi.org/10.1523/JNEUROSCI.15-11-07079.1995

Maurer, A. P., Burke, S. N., Lipa, P., Skaggs, W. E., & Barnes, C. A. (2012). Greater running speeds result in altered hippocampal phase sequence dynamics. *Hippocampus*, *22*(4), 737–747. https://doi.org/10.1002/hipo.20936

McNaughton, B. L., Barnes, C. A., & O'Keefe, J. (1983). *The contributions of position, direction, and velocity to single unit activity in the hippocampus of freely-moving rats*. *52*, 41–49. https://doi.org/10.1007/BF00237147

McNaughton, L., Chen, L. L., & Markus, J. (1991). "Dead Reckoning," Landmark Learning, and the Sense of Direction: A Neurophysiological and Computational Hypothesis. *Journal of Cognitive Neuroscience*, *3*(2), 190–202.

Moelands, A., & Schutte, H. (n.d.). *Two-wire bus-system comprising a clock wire and a data wire for interconnecting a number of stations* (Patent No. 4,689,740).
Moita, M. A. P., Rosis, S., Zhou, Y., LeDoux, J. E., & Blair, H. T. (2003). Hippocampal Place Cells Acquire Location-Specific Responses to the Conditioned Stimulus during Auditory Fear Conditioning. *Neuron*, *37*(3), 485–497. https://doi.org/10.1016/S0896-6273(03)00033-3
Muller, R., Bostock, E., Taube, J., & Kubie, J. (1994). On the directional firing properties of hippocampal place cells. *The Journal of Neuroscience*, *14*(12), 7235–7251. https://doi.org/10.1523/JNEUROSCI.14-12-07235.1994
Navratilova, Z., Hoang, L. T., Schwindel, C. D., Tatsuno, M., & McNaughton, B. L. (2012). Experience-dependent firing rate remapping generates directional selectivity in hippocampal place cells. *Frontiers in Neural Circuits*, *6*, 1–14. https://doi.org/10.3389/fncir.2012.00006
Nitz, D. A. (2012). Spaces within spaces: Rat parietal cortex neurons register position across three reference frames. *Nature Neuroscience*, *15*(10), 1365–1367. https://doi.org/10.1038/nn.3213
O'Keefe, J. (1976). Place units in the hippocampus of the freely moving rat. *Experimental Neurology*, *51*(1), 78–109. https://doi.org/10.1016/0014-4886(76)90055-8
O'Keefe, J., & Burgess, N. (1996). Geometric determinants of the place fields of hippocampal neurons. *Nature*, *381*(6581), 425–428. https://doi.org/10.1038/381425a0
O'Keefe, J., & Dostrovsky, J. (1971). The hippocampus as a spatial map. Preliminary evidence from unit activity in the freely-moving rat. *Brain Research*, *34*(1), 171–175. https://doi.org/10.1016/0006-8993(71)90358-1
O'Keefe, J., & Nadel, L. (1978). *The hippocampus as a cognitive map*. Clarendon Press ; Oxford University Press.
Olson, J. M., Tongprasearth, K., & Nitz, D. A. (2017). Subiculum neurons map the current axis of travel. *Nature Neuroscience*, *20*(2), 170–172. https://doi.org/10.1038/nn.4464
Park, E., Dvorak, D., & Fenton, A. A. (2011). Ensemble Place Codes in Hippocampus: CA1, CA3, and Dentate Gyrus Place Cells Have Multiple Place Fields in Large Environments. *PLoS ONE*, *6*(7), e22349. https://doi.org/10.1371/journal.pone.0022349
Pastalkova, E., Itskov, V., Amarasingham, A., & Buzsaki, G. (2008). Internally Generated Cell Assembly Sequences in the Rat Hippocampus. *Science*, *321*(5894), 1322–1327. https://doi.org/10.1126/science.1159775
Pedregosa, F., Varoquaux, G., Gramfort, A., Michel, V., Thirion, B., Grisel, O., Blondel, M., Prettenhofer, P., Weiss, R., Dubourg, V., Vanderplas, J., Passos, A., Cournapeau, D., Brucher, M., Perrot, M., & Duchesnay, E. (2011). Scikit-learn: Machine Learning in Python. *Journal of Machine Learning Research*, *12*, 2825–2830.
R Core Team. (2020). *R: A Language and Environment for Statistical Computing*. R Foundation for Statistical Computing. https://www.R-project.org/
Rich, P. D., Liaw, H.-P., & Lee, A. K. (2014). Large environments reveal the statistical structure governing hippocampal representations. *Science*, *345*(6198), 814–817. https://doi.org/10.1126/science.1255635
Rubin, A., Yartsev, M. M., & Ulanovsky, N. (2014). Encoding of Head Direction by Hippocampal Place Cells in Bats. *The Journal of Neuroscience*, *34*(3), 1067–1080. https://doi.org/10.1523/JNEUROSCI.5393-12.2014
Savelli, F., Yoganarasimha, D., & Knierim, J. J. (2008). Influence of boundary removal on the spatial representations of the medial entorhinal cortex. *Hippocampus*, *18*(12), 1270–1282. https://doi.org/10.1002/hipo.20511
Savelli, F., Luck, J., & Knierim, J. J. (2017). Framing of grid cells within and beyond navigation boundaries. *ELife*, *6*, e21354. https://doi.org/10.7554/eLife.21354
Seabold, S., & Perktold, J. (2010). statsmodels: Econometric and statistical modeling with python. *9th Python in Science Conference*.

Shapiro, M. L., Tanila, H., & Eichenbaum, H. (1997). Cues that hippocampal place cells encode: Dynamic and hierarchical representation of local and distal stimuli. *Hippocampus*, *7*(6), 624–642. https://doi.org/10.1002/(SICI)1098-1063(1997)7:6<624::AID-HIPO5>3.0.CO;2-E

Sharp, P. E. (1999). Subicular place cells expand or contract their spatial firing pattern to fit the size of the environment in an open field but not in the presence of barriers: Comparison with hippocampal place cells. *Behavioral Neuroscience*, *113*(4), 643–662. https://doi.org/10.1037/0735-7044.113.4.643

Singer, A. C., Karlsson, M. P., Nathe, A. R., Carr, M. F., & Frank, L. M. (2010). Experience-Dependent Development of Coordinated Hippocampal Spatial Activity Representing the Similarity of Related Locations. *Journal of Neuroscience*, *30*(35), 11586–11604. https://doi.org/10.1523/JNEUROSCI.0926-10.2010

Skaggs, W. E., & McNaughton, B. L. (1998). Spatial Firing Properties of Hippocampal CA1 Populations in an Environment Containing Two Visually Identical Regions. *The Journal of Neuroscience*, *18*(20), 8455–8466. https://doi.org/10.1523/JNEUROSCI.18-20-08455.1998

Solstad, T., Boccara, C. N., Kropff, E., Moser, M.-B., & Moser, E. I. (2008). Representation of Geometric Borders in the Entorhinal Cortex. *Science*, *322*(5909), 1865–1868. https://doi.org/10.1126/science.1166466

Spiers, H. J., Hayman, R. M. A., Jovalekic, A., Marozzi, E., & Jeffery, K. J. (2015). Place Field Repetition and Purely Local Remapping in a Multicompartment Environment. *Cerebral Cortex*, *25*(1), 10–25. https://doi.org/10.1093/cercor/bht198

Stewart, S., Jeewajee, A., Wills, T. J., Burgess, N., & Lever, C. (2014). Boundary coding in the rat subiculum. *Philosophical Transactions of the Royal Society B: Biological Sciences*, *369*(1635), 20120514. https://doi.org/10.1098/rstb.2012.0514

Taube, J. S. (1998). Head direction cells and the neurophysiological basis for a sense of direction. *Progress in Neurobiology*, *55*(3), 225–256. https://doi.org/10.1016/S0301-0082(98)00004-5

Tsao, A., Sugar, J., Lu, L., Wang, C., Knierim, J. J., Moser, M.-B., & Moser, E. I. (2018). Integrating time from experience in the lateral entorhinal cortex. *Nature*, *561*(7721), 57–62. https://doi.org/10.1038/s41586-018-0459-6

van der Walt, S., Schönberger, J. L., Nunez-Iglesias, J., Boulogne, F., Warner, J. D., Yager, N., Gouillart, E., & Yu, T. (2014). scikit-image: Image processing in Python. *PeerJ*, *2*, e453. https://doi.org/10.7717/peerj.453

Virtanen, P., Gommers, R., Oliphant, T. E., Haberland, M., Reddy, T., Cournapeau, D., Burovski, E., Peterson, P., Weckesser, W., Bright, J., van der Walt, S. J., Brett, M., Wilson, J., Millman, K. J., Mayorov, N., Nelson, A. R. J., Jones, E., Kern, R., Larson, E., … Vázquez-Baeza, Y. (2020). SciPy 1.0: Fundamental algorithms for scientific computing in Python. *Nature Methods*, *17*(3), 261–272. https://doi.org/10.1038/s41592-019-0686-2

Wiebe, S. P., & Stäubli, U. V. (1999). Dynamic Filtering of Recognition Memory Codes in the Hippocampus. *The Journal of Neuroscience*, *19*(23), 10562–10574. https://doi.org/10.1523/JNEUROSCI.19-23-10562.1999

Wiener, S., Paul, C., & Eichenbaum, H. (1989). Spatial and behavioral correlates of hippocampal neuronal activity. *The Journal of Neuroscience*, *9*(8), 2737–2763. https://doi.org/10.1523/JNEUROSCI.09-08-02737.1989

Wilson, M., & McNaughton, B. (1993). Dynamics of the hippocampal ensemble code for space. *Science*, *261*(5124), 1055–1058. https://doi.org/10.1126/science.8351520

Wood, E. R., Dudchenko, P. A., & Eichenbaum, H. (1999). The global record of memory in hippocampal neuronal activity. *Nature*, *397*(6720), 613–616. https://doi.org/10.1038/17605

Wood, E. R., Dudchenko, P. A., Robitsek, R. J., & Eichenbaum, H. (2000). Hippocampal Neurons Encode Information about Different Types of Memory Episodes Occurring in the Same Location. *Neuron*, *27*(3), 623–633. https://doi.org/10.1016/S0896-6273(00)00071-4

Zeileis, A., & Hothorn, T. (2002). Diagnostic Checking in Regression Relationships. *R News*, *2*(3), 7–10.

Ziv, Y., Burns, L. D., Cocker, E. D., Hamel, E. O., Ghosh, K. K., Kitch, L. J., Gamal, A. E., & Schnitzer, M. J. (2013). Long-term dynamics of CA1 hippocampal place codes. *Nature Neuroscience*, *16*(3), 264–266. https://doi.org/10.1038/nn.3329